Research Square

Preprints are preliminary reports that have not undergone peer review.
They should not be considered conclusive, used to inform clinical practice,
or referenced by the media as validated information.

Genome-resolved multi-omics characterization of Lentilactobacillus buchneri subsp. silagei strain AGA55 from Turkish shalgam: taxogenomics, safety, and probiotic-functional potential

Ahmet Yetiman

ahmetyetiman@erciyes.edu.tr

Erciyes University

Research Article

Keywords: multi-omics, probiotic, antibiotic-resistance, cholesterol, antioxidant, anti-cancer

Posted Date: July 3rd, 2026

DOI: https://doi.org/10.21203/rs.3.rs-10004860/v1

License: This work is licensed under a Creative Commons Attribution 4.0 International License.
Read Full License

Additional Declarations: No competing interests reported.

Genome-resolved multi-omics characterization of *Lentilactobacillus buchneri* subsp. *silagei* strain AGA55 from Turkish shalgam: taxogenomics, safety, and probiotic-functional potential

Ahmet E. YETİMAN[1*]

[1] Food Engineering Department, Faculty of Engineering, Erciyes University, 38030, Kayseri, Turkiye

*Corresponding author: ahmetyetiman@erciyes.edu.tr

Phone: +90 352 207 6666/ Ext: 32732

ORCID ID: 0000-0001-8406-7226

Abstract

Lentilactobacillus buchneri subsp. silagei strain AGA55, isolated from traditional Turkish lactic acid fermented shalgam juice, was characterized using an integrated, genome-resolved multi-omics approach. Taxogenomic analyses based on average nucleotide identity (ANI) and digital DNA–DNA hybridization (dDDH) confirmed its subspecies assignment and resolved at least two genomically distinct subgroups within the *Llb. buchneri* complex. A pangenome analysis of 27 strains, including AGA55, revealed an open architecture indicative of considerable genomic plasticity. The mobilome reinforced this view, comprising two intact prophage-like regions and a diverse insertion-sequence repertoire consistent with active horizontal gene transfer. Antimicrobial resistance determinants, identified phenotypically and in silico, were exclusively chromosomal and intrinsic, with no transferable elements detected, indicating a favorable safety profile. In vitro characterization supported strong probiotic potential, with high auto-aggregation (81.60%), robust survival under simulated gastrointestinal conditions, and acceptable antimicrobial activity. The strain showed potent DPPH (73,14±0,81%) and $ABTS^{+}$ (73,03±0,26%) radical-scavenging activity, corroborated genomically by a multi-tiered oxidative-stress defense repertoire and metabolomically by organic acids, polyols, and the cyclic dipeptide cyclo(L-Pro-L-Leu) in the cell-free supernatant. Moderate cholesterol assimilation (37,04±2,08 %) aligned with genomic evidence for bile salt hydrolase and mevalonate-pathway enzymes. The cell-free supernatant exerted concentration-dependent cytotoxicity against HT-29 and DLD-1 colorectal adenocarcinoma cells (IC_{50} 8.55 and 3.44 mg/mL, respectively), with DLD-1 showing greater sensitivity. Fermentation profiling confirmed an obligately heterofermentative metabolism and broad utilization of plant-derived substrates. Collectively, these findings establish AGA55 as a metabolically versatile strain with notable probiotic and biotechnological potential, warranting further in vivo investigation.

Keywords: multi-omics, probiotic, antibiotic-resistance, cholesterol, antioxidant, anti-cancer

Introduction

Lactic acid bacteria (LAB) constitute a functionally diverse group of Gram-positive, catalase-negative microorganisms that occupy a broad range of ecological niches, from fermented foods and plant material to the gastrointestinal tract (Douillard and de Vos 2014; Duar et al. 2017; Yetiman 2025). During fermentation, their metabolic activity reaches well beyond simple acidification. These bacteria produce organic acids, bacteriocins, exopolysaccharides, and a range of bioactive metabolites that together shape the safety, quality, and functional value of the final product (Douillard and de Vos 2014; Yetiman et al. 2022, 2024, 2026). Importantly, the recent reclassification of the former genus Lactobacillus into 25 genera, 23 of them newly described, has established a taxonomically resolved framework for examining the ecological and metabolic specialization of individual lineages (Zheng et al. 2020).

Shalgam is a traditional Turkish lactic-acid-fermented beverage prepared from purple carrot, turnip, bulgur flour, and salt (Yetiman et al. 2022). Earlier work has shown that shalgam-derived LAB strains possess a range of functionally relevant properties, including cholesterol reduction, GABA production, antimicrobial activity, antioxidant capacity, and cytotoxicity toward colorectal cancer cell lines (Ekinci et al. 2016; Yetiman et al. 2024, 2026). Taken together, these findings identify shalgam as a rich reservoir of functionally diverse LAB strains with promising applications in food and health.

Lentilactobacillus buchneri (Llb. buchneri) is an obligately heterofermentative LAB species distributed widely across silage, fermented plant materials, and food-related environments (Heinl et al. 2012; Heinl and Grabherr 2017; Irimajiri et al. 2024). This species is distinguished by a notable metabolic capacity: under anaerobic, acidic conditions, it converts lactic acid into acetic acid and 1,2-propanediol, a pathway that helps sustain cell viability during the later stages of fermentation (Oude Elferink et al. 2001; Tanizawa et al. 2020). The accumulating acetic acid, in turn, improves the aerobic stability of silage by suppressing mold and yeast proliferation, which makes *Llb. buchneri* a valuable inoculant in agricultural silage production (Danner et al. 2003; Liu et al. 2011). Its genome encodes a versatile metabolic repertoire that spans diverse carbohydrate transport and utilization systems, stress-response mechanisms, and secondary metabolite biosynthesis gene clusters (Heinl et al. 2012). Within this species, the subspecies *Llb. buchneri* subsp. *silagei*, formally described by Tanizawa et al. (2020), forms a phylogenetically distinct clade isolated primarily from rice-grain silage environments. To date, only a limited number of *Llb. buchneri* subsp. *silagei* genomes have been deposited in NCBI (Liu et al. 2011; Tanizawa et al. 2020; Irimajiri et al. 2024), and their probiotic-associated genomic and phenotypic features have yet to be systematically examined within a multi-omics framework.

Pangenome analysis has become an indispensable tool for characterizing bacterial species at the population level, allowing researchers to delineate core and accessory genomic content and to detect strain-specific metabolic specialization (Tettelin et al. 2005, 2008). For food-related and probiotic LAB in particular, comparative genomic approaches have proven crucial in identifying genes that govern carbohydrate metabolism, stress resilience, and host interactions (Makarova et al. 2006; Douillard and de Vos 2014). Integrating comparative genomics with in vitro phenotypic characterization, metabolite profiling, and cytotoxicity assays, therefore, offers a comprehensive strategy

for evaluating both the safety and the functional potential of candidate probiotic strains (Yetiman et al. 2024, 2026; Kim et al. 2026; Liu et al. 2026).

The present study aimed to address this gap by providing a genome-resolved, multi-omics characterization of *Llb. buchneri* subsp. *silagei* strain AGA55, isolated from commercially available Turkish shalgam juice. Specifically, our objectives were to (i) determine the taxogenomic position of AGA55 using ANI and dDDH analyses; (ii) assess its pangenomic relationship within the *Llb. buchneri* species; (iii) characterize its mobilome, resistome, and secondary metabolite gene clusters; (iv) evaluate its carbohydrate-metabolic potential through combined genomic and phenotypic approaches; and (v) systematically investigate its probiotic-relevant traits, including antioxidant activity, cholesterol assimilation, gastrointestinal survival, antimicrobial activity, and cytotoxicity against HT-29 and DLD-1 colorectal cancer cell lines.

Materials and Methods

Isolation and Cultivation Parameters

Llb. buchneri subsp. silagei strain AGA55 was recovered from a commercially available Turkish shalgam juice (pH 3.01) obtained from a regional producer (Doktorum Yılmaz, Adana, Türkiye). For primary isolation, a 10 mL sample was diluted tenfold in 90 mL of sterile physiological saline (0.85%, w/v) and homogenized by vortexing for 1 min on an MS-3 Basic vortex mixer (IKA-Werke GmbH, Staufen, Germany). Serial decimal dilutions were then prepared, and 100 µL aliquots of each were spread onto MRS agar (Merck GmbH, Darmstadt, Germany). The plates were incubated under strictly anaerobic conditions at 30 °C for 5 days. A morphologically representative colony from the 10^{-5} dilution was selected, designated AGA55, and purified through two successive streak-plating cycles to ensure an axenic culture. Isolate identity and purity were preliminarily verified by Gram staining and a catalase test. For long-term storage, cryoprotective stocks were prepared by resuspending cells in MRS broth (Merck) supplemented with 25% (v/v) glycerol, and these were maintained at −80 °C until further use.

DNA Extraction, Whole-Genome-Sequencing, and Assembly

Prior to DNA extraction, the AGA55 cryostock was revitalized through two sequential subculture passages in MRS broth (Merck) under anaerobic conditions at 37 °C for 24 h. Cells were harvested from 1 mL of an actively growing culture by centrifugation at 6,000 × g for 10 min at 4 °C in sterile 2 mL microcentrifuge tubes. Genomic DNA was then extracted using the PureLink Genomic DNA Mini Kit (Invitrogen, Thermo Fisher Scientific, Carlsbad, CA, USA), according to the manufacturer's recommended protocol for Gram-positive bacteria. The concentration, purity, and integrity of the extracted DNA were assessed using a Qubit 3.0 fluorometer (Invitrogen, Thermo Fisher Scientific) in conjunction with an Agilent 5400 Fragment Analyzer. Sequencing libraries were constructed with the Nextera XT DNA Library Preparation Kit (Illumina, USA) and subsequently purified using AMPure XP magnetic beads (Beckman Coulter, UK) according to the manufacturer's specifications. Whole-genome sequencing was carried out on an Illumina NovaSeq 6000 platform employing a 2 × 150 bp paired-end read configuration, and raw sequencing data were retrieved in compressed FASTQ format (fastq.gz). De novo genome assembly was performed using Shovill (v1.1.0) via the

Galaxy Europe web server (https://usegalaxy.eu/). Assembly completeness was evaluated with CheckM, which confirmed 100% genome completeness.

Bioinformatic analyses

The NCBI Prokaryotic Genome Annotation Pipeline (PGAP) was utilized for genome annotation (Tatusova et al. 2016). Additionally, RASTtk and BV-BRC annotations were performed for comparison with PGAP (Brettin et al. 2015; Olson et al. 2023). The genome of *Llb. buchneri* AGA55 was compared with metagenome-assembled genomes (MAGs) from JGI-IMG/MER(Chen et al. 2023). The genome data package used in this study was downloaded from the NCBI website (Taxon ID: 1581). BRIG v1.1.0 (https://sourceforge.net/projects/brig/) was employed to generate a BLAST Ring Image of the AGA55 strain's genome and those of other comparable *Llb. buchneri* strains (Alikhan et al. 2011). Before pangenome analysis, all *Llb. buchneri* genomes in this study were merged into a single contig and annotated using Prokka (v.1.14.5) (Seemann 2014). Pangenome analysis was conducted with Pan-genome Explorer and the PanACoTA comparative genomics tool, with a minimum identity threshold of 80% (Perrin and Rocha 2021; Dereeper et al. 2022). The fastANI algorithm calculated average nucleotide identity (ANI) values for AGA55 and other similar *Llb. buchneri* strains (Jain et al. 2018). Digital DNA-DNA hybridization (dDDH) analyses were performed using DSMZ's web interface for the genome-to-genome distance calculator (Meier-Kolthoff et al. 2022). The dbCAN3 meta-server was used to predict CAZymes (Zheng et al. 2023). For metabolic pathway analysis, *Llb. buchneri* AGA55's genome was scanned against the KEGG database using BlastKOALA (Kanehisa et al. 2016). Furthermore, MetaCyc-based metabolic pathway screening was performed through JGI-IMG/MER (Chen et al. 2023). Resistome screening involved examining the entire genome sequence of AGA55 through the BV-BRC and KEGG databases. Clusters of Ortholog Groups (COGs) were identified from the genome set used in this study through functional sequence annotation by orthology using eggNOG Mapper (Galaxy Version 2.1.8+galaxy4) (Huerta-Cepas et al. 2017, 2019). Protein-coding genes associated with antibiotic resistance were screened against the NCBI non-redundant protein (NR) database using protein-BLAST. The genes with homologous proteins that are at least 80% identical to those of bacteria other than *Llb. buchneri* were considered to have undergone horizontal gene transfer. Data visualization, including heatmap generation, was performed in the RStudio environment (R Core Team 2024). The metabolic overview of carbohydrate metabolism was illustrated using PathVisio V.3.30 (Kutmon et al. 2015). The genome sequence has been deposited in NCBI under the accession numbers BioSample: SAMN47207974 and NZ_CP183391.

Determination of antibiotic susceptibility

The antibiotic susceptibility of strain AGA55 was evaluated using antibiogram assays to determine its resistance or sensitivity to commonly used antimicrobials. Susceptibility testing of *Llb. buchneri* sp. *silagei* AGA55 was conducted with ready-to-use commercial antibiotic discs, including Methicillin (5 µg), Penicillin G (10 U), Streptomycin (10 µg), Amikacin (30 µg), Kanamycin (30 µg), Vancomycin (30 µg), Azithromycin (15 µg), Erythromycin (10 µg), and Tetracycline (30 µg) (Bioanalyse, Ankara, Türkiye). The disk diffusion procedure was performed according to the Kirby–Bauer method (Khan et al. 2019). Inhibition zone diameters (mm) were measured and interpreted in accordance with the Clinical and Laboratory Standards Institute (CLSI) performance standards for antimicrobial susceptibility testing.

Analysis of cell-free supernatants using GC-MS

The freeze-dried cell-free supernatant (CFS) of the AGA55 was chemically derivatized prior to GC-MS analysis. CFS was dissolved only in Acetonitrile. Derivatization and GC-MS analysis were performed as described by Yetiman et al. (2026) (Yetiman et al. 2026). After analysis, the identified compounds were verified by matching them with data from the WILEY-NIST (12th Edition, 2020) GC–MS spectral database.

Cytotoxicity versus HT29 and DLD-1 cell lines

The cytotoxic activity of bacterial cell-free supernatants was evaluated using human colon cancer cell lines HT-29 and DLD-1. Cell viability was measured through the colorimetric CCK-8 (Cell Counting Kit-8, MedChemExpress, NJ, USA) assay, as previously described by Bouhlel et al. (2026) (Bouhlel et al. 2026).

Carbohydrate fermentation tests

The carbohydrate fermentation profiles of the AGA55 strain were assessed using an API 50 CH kit (BioMérieux, Marcy-l'étoile, France), comprising 49 carbohydrate assays, according to the manufacturer's instructions. Test results were compared with those of other *Lentilactobacillus* members using the API test finder from the BacDive website (https://bacdive.dsmz.de/api-test-finder), depicted as a heatmap (Reimer et al. 2019).

Examination of Probiotic Features

Hemolytic potential of *Lentilactobacillus buchneri* subsp. *silagei* AGA55 was evaluated on blood agar containing 5% (v/v) defibrinated sheep blood. A fresh culture was streaked onto plates and incubated under anaerobic conditions (typically at 37 °C for 24–48 h). Hemolysis was recorded by visual inspection of the colonies and surrounding medium and classified as β-hemolysis (clear zones), α-hemolysis (greenish discoloration), or γ-hemolysis (no halo), with γ-hemolysis interpreted as the absence of detectable hemolytic activity. The auto-aggregation assay was performed according to the method described by Maione et al. (2024) with minor modifications (Maione et al. 2024). Cell-surface hydrophobicity was determined by measuring adhesion to xylene with respect to Yetiman et al (2024)(Yetiman et al. 2024). The antimicrobial activity of the cell-free supernatant (CFS) was assessed using the agar well diffusion method (Haghshenas et al. 2023). The CFS was tested versus *Escherichia coli* O157:H7 ATCC 43897, *Escherichia coli* ATCC 25922, *Staphylococcus aureus* ATCC 25923, *Bacillus cereus* ATCC 33019, and *Klebsiella pneumoniae* ATCC 11883. In vitro static gastrointestinal simulation was conducted using the INFOGEST protocol (Brodkorb et al. 2019), as modified by Yetiman (2025) (Yetiman 2025).

Antioxidant activity and Cholesterol assimilation assays

The antioxidant activity of cell-free supernatants of AGA55 was evaluated using DPPH (2,2-diphenyl-1-picrylhydrazyl) and ABTS+ (2,2'-azino-bis(3-ethylbenzothiazoline-6-sulfonic acid)) radicals. Antioxidant activity and cholesterol assimilation assays were performed following the protocol described by Yetiman et. al. (2026) (Yetiman et al. 2026).

Results and Discussion

Taxogenomics of *Len. buchneri* subsp. *silagei* strain AGA55

The genome of AGA55, annotated with GeneMarkS-2+ using the best-placed reference protein set (NCBI), consists of a single circular chromosome measuring 2,594,120 base pairs and with a GC content of 43.98%. It encodes 2,574 genes, including 2,442 protein-coding sequences, 53 tRNA genes, one copy each of 5S, 16S, and 23S rRNA, three non-coding RNA genes, 73 pseudogenes, and one CRISPR array with its respective type-II Cas proteins (Cas1, Cas2, Csn2, and Cas9). Additionally, Table 1 summarizes genomic statistics and quality metrics. The genomic architecture of AGA55 aligns with that of other members of the *Lentilactobacillus* genus (Heinl et al. 2012; Zheng et al. 2020; Tanizawa et al. 2020; Irimajiri et al. 2024), yet its distinctive gene content points to specialized adaptations for thriving in the particular ecological setting of traditional lactic acid fermented Turkish shalgam fermentation. The BRIG analysis (Alikhan et al. 2011) offers a clear visualization of the genomic regions conserved between AGA55 and representative strains from both clusters (Fig. 1). This alignment reveals striking synteny and conservation across much of the chromosome, while localized variations within genomic islands mark the critical points of difference. Such islands can be reliably distinguished from the surrounding chromosome by their characteristic nucleotide signatures, including shifts in GC content, cumulative GC skew, tetranucleotide frequencies, and codon usage (Juhas et al. 2009). Frequently flanked by mobile genetic elements such as insertion sequences and transposases, these variable regions are likely key contributors to the unique metabolic capabilities and ecological adaptations of AGA55, among them its distinctive carbohydrate fermentation profile and probiotic traits (Yetiman et al. 2024).

The dDDH values provide a robust metric for species delineation, with values ≥70% typically indicating membership within the same species (Meier-Kolthoff et al. 2013, 2022). The DNA-DNA hybridization (dDDH) analysis conclusively demonstrates that AGA55 shares an exceptionally high genetic similarity, with dDDH values surpassing 96% in comparison to several reference genomes, including MGR2_32, S58, S59, NK01, 177, CIRM_BIA_1516, CIRM_BIA_2081, CIRM_BIA_1514, and SG162 (Table 2). These results, supported by narrow confidence intervals and high probabilities of DDH ≥70% (97.44%-97.83%), clearly indicate that AGA55 belongs to the same species as the reference strains.

Notably, the dDDH values showed a distinct bimodal distribution when comparing AGA55 to 26 *Llb. buchneri* genomes. A cluster of nine strains (MGR2_32, S58, S59, NK01, 177, CIRM_BIA_1516, CIRM_BIA_2081, CIRM_BIA_1514, and SG162) exhibited dDDH values ranging from 96.0% to 97.9%, with corresponding genetic distances between 0.0033 and 0.0055. This tight clustering suggests these strains represent the same subspecies (*Llb. buchneri* sp. *silagei*) or highly conserved clade within *Llb. buchneri*. In contrast, a second group comprising 17 strains (MGB0786, RUG14303, ATCC4005, PC-C1, CIRM_BIA_2083, 1014, DSM20057, CIRM_BIA_664, CIRM_BIA_845, CIRM_BIA_2084, LA1184, CIRM_BIA_2082, LA1167, LA1147, LA1161B, FUA3252, and 1012) showed dDDH values between 75.8% and 78.1%, with genetic distances ranging from 0.0257 to 0.0284. These values, while still above the 70% species threshold, indicate substantial genomic divergence and likely represent distinct subspecies or ecotypes within *Llb. buchneri*. The GC content difference between AGA55 and the compared genomes

was minimal, ranging from 0.00% to 0.60%, with most comparisons showing differences ≤0.36%. This narrow range of GC content variation further supports the close phylogenetic relationship among these strains while highlighting subtle genomic adaptations that may underlie phenotypic differences in carbohydrate metabolism and stress tolerance observed in subsequent analyses.

Average nucleotide identity (ANI) analysis, performed with the FastANI algorithm (Jain et al. 2018), complemented the dDDH findings. AGA55 shared ANI values exceeding 99% with members of the high-dDDH cluster (the silagei cluster), confirming their close genomic relatedness. As shown in Fig. 2, most members of this cluster originated from silage and bovine nasopharynx, the exceptions being AGA55 (shalgam) and CIRM-BIA-2081 (grape must). A closer look at the ANI phylogram in the same figure suggests that the partial differences in genetic distance among the genomes of the *Llb. buchneri* and *Llb. buchneri* subsp. *silagei* clusters can be largely attributed to their distinct or shared isolation niches, evolutionary trajectories, and environmental exposures (Heinl and Grabherr 2017; Nethery et al. 2019; Rodriguez-R et al. 2023). These differences appear to be driven most strongly by the adaptable, free-living lifestyle of *Llb. buchneri* across a wide range of niches (Duar et al. 2017; Nethery et al. 2019). For the second cluster, ANI similarity with AGA55 ranged from 97% to 97.38%. These values remained above the 95–96% species boundary yet still reflected the genomic divergence observed in the dDDH analysis (Richter and Rosselló-Móra 2009; Meier-Kolthoff et al. 2013; Karaman et al. 2025). This combination of high ANI (>96%) and dDDH values exceeding 70% across all comparisons unambiguously places AGA55 within *Llb. buchneri* subsp. *silagei*. The bimodal distribution, moreover, points clearly to the existence of at least two distinct genomic subgroups within this species complex. Collectively, the genomic features of AGA55, particularly its high dDDH and ANI values relative to the reference strains, confirm its taxonomic assignment to *Llb. buchneri* subsp. *silagei* while underscoring both its free-living lifestyle and its distinct genomic signature.

Pangenome Analysis

Pangenome analysis identified 5,226 gene clusters, which were sorted into core, dispensable, and strain-specific (singleton) categories according to their distribution across the analyzed strains (Fig. 3A). The core genome, those genes shared by all 27 *Llb. buchneri* strains, comprised 1,725 gene clusters, or 33.0% of the total pangenome. These conserved genes encode the essential housekeeping functions that underpin fundamental cellular activity, including central metabolism, DNA replication, transcription, translation, and cell-envelope biosynthesis. They may also harbor genes that set one species apart from others within the same genus (Mosquera-Rendón et al. 2016; Yetiman et al. 2025).

The dispensable genome, made up of genes present in some but not all strains, contained 1,741 gene clusters and accounted for 33.3% of the pangenome. Of these, 180 genes (3.44% of the total) were shared among 26 strains; these accessory genes may confer adaptive advantages in particular ecological niches (Tettelin et al. 2008; Duar et al. 2017). The remaining 1,760 genes (33.7%) were strain-specific singletons, underscoring the substantial genomic diversity within the species. Such a high proportion of strain-specific genes points to extensive horizontal gene transfer and considerable genomic plasticity, traits that likely help *Llb. buchneri* adapt to the diverse conditions it encounters across different fermentation ecosystems (Juhas et al. 2009; Duar et al. 2017; Heinl and Grabherr 2017; Nethery et al. 2019).

The calculated α-value of 0.594, obtained through the Heaps' law approach (Tettelin et al. 2005, 2008), denotes an open pangenome ($\alpha < 1$). Consistent with this, the rarefaction curve (Fig. 3B) follows a logarithmic trajectory rather than reaching a plateau, implying that the sequencing of additional genomes would likely uncover further gene clusters. Such openness indicates that *Llb. buchneri* retains considerable genomic plasticity and continues to acquire new genes through horizontal gene transfer, a pattern that aligns well with its free-living lifestyle and its adaptation to diverse fermentation environments (Juhas et al. 2009; Duar et al. 2017).

Hierarchical clustering of gene presence/absence patterns (Fig. 4) revealed two distinct genomic groups corresponding to the previously identified dDDH/ANI clusters: the *L. buchneri sp. silagei* clade (including AGA55, MGR2_32, S58, S59, NK01, 177, CIRM_BIA_1516, CIRM_BIA_2081, CIRM_BIA_1514, and SG162) and the broader *L. buchneri* group. The Upset plot visualization (Fig. 5) further illustrated the intersection patterns of gene clusters across strains, highlighting both shared core genes and strain-specific genomic features.

Functional annotation based on the Clusters of Orthologous Groups (COG) classification revealed distinct patterns in how gene functions were distributed across the core and accessory genomes (Fig. 6). Within the core genome, genes were enriched in COG categories J (translation, ribosomal structure and biogenesis; 129 genes), E (amino acid transport and metabolism; 263 genes), G (carbohydrate transport and metabolism; 103 genes), K (transcription; 131 genes), and L (replication, recombination and repair; 118 genes). These categories encompass the fundamental cellular processes that bacteria depend on for survival and growth across diverse environments. The accessory genome, by contrast, was enriched in categories tied to environmental adaptation and niche specialization. Here, category S (function unknown) accounted for the largest share of accessory genes (463 genes in AGA55), followed by categories E (amino acid transport and metabolism; 215 genes), G (carbohydrate transport and metabolism; 177 genes), and K (transcription; 183 genes). The strong representation of category S in the accessory genome suggests that many strain-specific adaptations rely on genes whose functions remain uncharacterized, genes that may encode novel metabolic capabilities or regulatory mechanisms suited to particular ecological niches.

The COG category heatmap (Fig. 7) offered a comprehensive overview of functional gene distribution across all 27 genomes, with the two genomic clusters separating clearly on the basis of their COG profiles. A closer analysis of singleton genes further revealed strain-specific patterns of functional specialization (Fig. 8). In AGA55, singletons fell mainly into categories K (transcription; 17 genes), L (replication, recombination, and repair; 35 genes), M (cell wall/membrane/envelope biogenesis; 11 genes), and S (function unknown; 2 genes). Notably, AGA55 carried no singleton genes in several categories (J, A, B, Y, Z, W, U, O, Q, R), indicating that its distinctive genetic repertoire centers on transcriptional regulation, DNA maintenance, and cell-envelope modification rather than on translation, RNA processing, or secondary metabolism.

The number of singleton genes varied markedly across the 27 genomes, ranging from 1 in strain CIRM_BIA_845 to 259 in strain 1012. On average, each strain contained 65.19 ± 57.3 singleton genes. Strain AGA55 harbored 100 singleton genes, indicating that it possesses a distinct, yet not excessively expanded, strain-specific gene repertoire. Compared with strains showing particularly large singleton sets, such as 1012, 1014, LA1147, and LA1184, AGA55 appears to maintain a relatively balanced genomic architecture. This pattern suggests that AGA55 combines a

conserved genomic background with a moderate set of unique genes that may contribute to strain-specific functional properties.

Strain-specific and accessory genes are central components of bacterial pangenomes, since they frequently reflect genome plasticity, niche adaptation, and functional diversification among closely related strains (Tettelin et al. 2005; Bonacina et al. 2017; Zhai and Wei 2022). In AGA55, a striking 78% of the singleton genes were annotated as hypothetical proteins. While their precise biological roles still await experimental validation, most could nonetheless be assigned to defined COG categories—an indication that they likely encode conserved yet poorly characterized proteins rather than entirely unknown products. COG classification, in this respect, provides a useful comparative framework for assigning predicted functions to orthologous protein groups and for interpreting functional categories across bacterial genomes (Tatusov et al. 2003). The hypothetical singletons of AGA55 were associated chiefly with replication, recombination, and repair; transcription; cell wall/membrane/envelope biogenesis; nucleotide transport and metabolism; and carbohydrate transport and metabolism. Taken together, this distribution suggests that the strain-specific gene pool of AGA55 may contribute to genome plasticity, regulatory flexibility, cell-surface remodeling, and metabolic adaptation.

Several annotated singleton genes further support the possible contribution of the AGA55-specific genome to probiotic-related traits. Genes encoding pyruvate oxidase, ribokinase, deoxyribose-phosphate aldolase, alcohol dehydrogenases, D-lactate/D-glycerate dehydrogenase, and putative carbohydrate transport functions, including fucose permease and isoprimeverose transporter (*xylP*), indicate a strain-specific capacity for carbohydrate utilization and organic acid-associated metabolism. Such functions are relevant because carbohydrate metabolism and substrate flexibility are central features of lactic acid bacteria's adaptation to food and fermentation environments (Douillard and de Vos 2014; Borowska et al. 2025). These features may enhance AGA55's ability to persist in nutrient-variable fermented food matrices. In addition, singleton genes encoding the DNA replication and repair protein *RecF*, DNA topoisomerase III, the divalent metal cation transporter *MntH*, the high-affinity heme uptake protein *IsdE*, and several transposase-related proteins suggest possible roles in genome maintenance, stress adaptation, metal ion homeostasis, nutrient acquisition, and genetic plasticity. The presence of singleton genes associated with cell wall, membrane, and envelope biogenesis is also biologically relevant, as bacterial surface structures can influence environmental persistence, host interaction, and probiotic-associated functionality. Previous comparative genomic studies of food-related and probiotic bacteria have also shown that accessory and hypothetical proteins may provide useful clues for niche specificity and functional characterization, although experimental validation remains necessary (Bonacina et al. 2017; Adejumo 2024). Therefore, although many AGA55-specific genes are currently annotated as hypothetical proteins, their COG distribution and associated annotated functions suggest that the singleton genome may contribute to the metabolic versatility, stress tolerance, and adaptive potential of AGA55 as a probiotic candidate.

Prophages and related mobilome

At first glance, the genome of *Llb. buchneri* subsp. *silagei* AGA55 contains two large prophage-like regions (Table 2). Region 1 spans 181,641–228,252 bp (46.6 kb; score 140; 66 proteins; GC 39.59%), whereas region 2 spans 2,048,245–2,101,764 bp (53.5 kb; score 150; 54 proteins; GC 38.32%). Both regions were classified as intact in the PHASTEST

web server. The PHASTEST database categorizes putative phage sites by score: intact (score > 90), incomplete (70-90), and questionable (< 70), depending on the extent of phage protein matching (Wishart et al. 2023). The identified phage regions were mainly linked to lactobacilli phages, especially PHAGE_Lactob_Lb_NC_047983, which shared 26 proteins in region 1 and 8 proteins in region 2. Notably, the detailed Supplemental Excel File shows 47 CDS for region 1 and 39 for region 2 in the phage-BLAST-hit tables, whereas Table 2 lists 66 and 54 total proteins for these regions. This discrepancy should be clarified, as the CDS-level export likely reflects only ORFs with phage-related matches, rather than the full set of predicted proteins in each region. The lower GC contents of the two predicted prophage regions compared with the overall chromosomal GC content of AGA55 are consistent with their phage-associated origin and possible acquisition through horizontal gene transfer; however, GC deviation should be interpreted as supportive rather than conclusive evidence and requires corroboration from gene content, synteny, and mobile-element context (Juhas et al. 2009; Langille et al. 2010).

At the gene level, both regions exhibit a modular organization compatible with intact-phage-derived genomic islands. Region 1 contains a putative tyrosine-type recombinase/integrase, a probable transcriptional repressor, XRE-family regulatory proteins, antirepressor-related proteins, a RecT recombinase, nuclease-like proteins, a helicase, small and large terminase subunits, a portal protein, head/capsid-associated proteins, baseplate-related proteins, lytic murein transglycosylase-associated proteins, and a GH25 family member lysozyme. Region 2 carries a repressor, helicase, AAA-family ATPase, bifunctional DNA primase/polymerase, N-6 DNA methylase, HNH endonuclease, terminase subunits, a portal protein, head maturation and capsid proteins, head-tail connector and closure proteins, multiple tail proteins including a tape-measure protein, a distal tail protein, and a tail spike protein, as well as a GH25 lysozyme, a holin-related protein, and a terminal site-specific integrase. Taken together, these features indicate that both regions retain gene sets typically associated with phage integration and recombination, DNA replication, genome packaging, virion morphogenesis, and host-cell lysis (Casjens 2003; Canchaya et al. 2004; Jarocki et al. 2023).

However, a cautious interpretation is required. No attachment-site annotations have been identified, and no clearly defined *attL* or *attR* junctions were observed. This is crucial mechanistically. In canonical temperate phage integration, the phage attachment site (*attP*) recombines with the bacterial attachment site (*attB*) to form the hybrid junctions *attL* and *attR*, which flank the integrated prophage. Therefore, identifying *attL* and *attR* strongly supports the presence of true chromosomal integration and helps delineate prophage boundaries (Raya et al. 1992; Merrick et al. 2018). Because there is no boundary evidence in the current phage dataset, it would be inappropriate to claim that these elements are definitively active lysogens or excisable prophages. Therefore, the most cautious interpretation is that AGA55 harbors two PHASTEST-predicted intact prophage-like regions whose gene content and organization are consistent with temperate-phage ancestry. However, this bioinformatic classification should not be taken as direct evidence of current excision capacity, inducibility, or production of infectious phage particles. In this context, the term “intact” refers to a sequence-based prediction derived from phage-related gene content, similarity to known phages, regional organization, and PHASTEST scoring criteria, rather than experimental confirmation of an active prophage lifecycle (Arndt et al. 2016a; Wishart et al. 2023). Interestingly, neither putative phage is flanked by the detected CRISPR array region (Table 1). Only region 1 has been observed roughly 50 kb upstream of the CRISPR array region. However, there is no evidence that the CRISPR array causes the loss of attachment sites.

The insertion-sequence profile further supports the view that the AGA55 mobilome has undergone notable structural remodeling. In total, 41 IS-associated hits were detected, with a marked predominance of the IS6 family (26/41), followed by IS30 (7), ISL3 (3), IS256 (2), IS3 (2), and IS21 (1). The highest-scoring matches included IS1310-, ISLpl1-, ISLsa1-, ISPp1-, IS153-, and IS1297-like elements, while many IS6-related homologs showed closest similarity to *Lactococcus lactis* ISS1-like elements (Supplemental Excel File). This IS-rich genomic background is relevant to the interpretation of the two PHASTEST-predicted prophage-like regions, because insertion sequences are major contributors to bacterial genome plasticity and can mediate insertional gene disruption, homologous recombination between repeated IS copies, deletions, inversions, and other local genome rearrangements (Mahillon and Chandler 1998; Siguier et al. 2014; Vandecraen et al. 2017). Importantly, IS elements have also been reported within prophage genomes, where they may interrupt prophage coding sequences and contribute to prophage fragmentation or loss of function (Vale et al. 2017). Such IS-associated disruption and rearrangement can therefore complicate the interpretation of prophage-like loci, especially because prophage identification and boundary assignment depend partly on genomic features such as integrase genes, direct repeats, and bacterial–phage attachment-site junctions (Fouts 2006; Arndt et al. 2016b). Therefore, the coexistence of two large prophage-like regions with a diverse IS repertoire is most consistent with a history of phage- and transposon-associated genome plasticity in AGA55.

Antimicrobial resistance profile and resistome

The antimicrobial susceptibility of *Llb. buchneri* subsp. *silagei* AGA55 was assessed phenotypically by disk diffusion, and inhibition zones were interpreted according to the Clinical and Laboratory Standards Institute (CLSI) guidelines (CLSI 2023). The phenotypic profile was then evaluated in parallel with genome-based resistome screening, since resistance traits in lactic acid bacteria intended for food- or probiotic-related applications may be either intrinsic and non-transferable or acquired and potentially transmissible (Ammor et al. 2007; EFSA-FEEDAP 2012). Accordingly, both the observed inhibition-zone patterns and the genomic context and taxonomic origin of the detected resistance-associated loci were considered in the interpretation.

Phenotypically, AGA55 was resistant to methicillin, streptomycin, amikacin, kanamycin, and vancomycin, with no measurable inhibition zones. Intermediate sensitivity was recorded against penicillin G (15.43 ± 0.33 mm) and azithromycin (15.63 ± 0.82 mm), whereas the strain was susceptible to erythromycin (22.16 ± 0.09 mm) and tetracycline (20.26 ± 0.30 mm) (Table 4). The aminoglycoside-resistant phenotype is consistent with the well-documented low susceptibility of lactobacilli to this class, which is generally attributed to intrinsic physiological traits, such as limited drug uptake during fermentative growth, rather than to acquired aminoglycoside-modifying enzymes (Ammor et al. 2007; Yetiman et al. 2024). The vancomycin-resistant phenotype is likewise commonly intrinsic in lactobacilli and reflects an altered peptidoglycan precursor in which the canonical D-Ala-D-Ala terminus is replaced by a lower-affinity D-Ala-D-Lac variant (Marshall et al. 1997; Yetiman et al. 2022).

In silico screening with BV-BRC and KEGG identified resistance-associated loci grouped into β-lactam and vancomycin categories. β-Lactam-associated hits included a predicted class A β-lactamase (*penP*), penicillin-binding protein genes (*pbp2A*, *mrcA*), an *AbcA*-type transporter, and an oligopeptide ABC transporter operon (*oppA–F*). These annotations are broadly consistent with the methicillin-resistant and penicillin-intermediate phenotypes observed for

AGA55, although penicillin-binding proteins and cell-wall biosynthetic enzymes are conserved chromosomal features of Gram-positive bacteria, and their presence alone does not establish acquired resistance (Ammor et al. 2007; Yetiman et al. 2024). The vancomycin category genes detected by KEGG (*Ddl, VanX, mraY, MurG, alr, MurF*) are mainly involved in peptidoglycan precursor synthesis, cell wall assembly, or D-alanine metabolism. Intrinsic vancomycin resistance is well documented in many lactobacilli and is commonly associated with naturally occurring peptidoglycan precursors terminating in D-Ala-D-Lac, which reduce vancomycin binding affinity (Goldstein et al. 2015; Yetiman et al. 2022, 2024). In the present genome, no complete canonical transferable *vanA*-, *vanB*-, or *vanC*-type cluster was detected, supporting the interpretation that the vancomycin-resistant phenotype of AGA55 is an intrinsic cell-wall-associated trait rather than evidence of a mobile glycopeptide-resistance operon (Reynolds 1989; Courvalin 2006).

K-mer-based AMR screening via BV-BRC identified 24 hits corresponding to 21 unique genes, most of which were classified as antibiotic targets in susceptible species rather than as acquired resistance determinants. Such target-based annotations require cautious interpretation, because BV-BRC/PATRIC AMR prediction may detect conserved loci associated with antimicrobial targets, and resistance involving these loci usually depends on specific mutations, altered expression, or acquired resistant alleles rather than the mere presence of the gene (Davis et al. 2016; Alcock et al. 2020; Olson et al. 2023). These included conserved targets of aminoglycosides, tetracyclines, rifamycins, fluoroquinolones, fosfomycin, sulfonamides, trimethoprim, cycloserine, fusidic acid, and mupirocin, such as *ef-Tu*, *ef-G*, *murA*, *rpsL* (S12p), *rpsJ* (S10p), *rpoB*, *rpoC*, *gyrA*, *gyrB*, *folA/Dfr*, *folP*, *kasA*, *inhA/fabI*, and *Iso-tRNA*. Because resistance mediated by such loci typically depends on specific mutations, altered expression, or acquired variant alleles rather than on the mere presence of the gene, these hits are not considered direct evidence of resistance in AGA55 (Campbell et al. 2001; Sköld 2001; Hooper and Jacoby 2015; Blair et al. 2015; Krause et al. 2016; Silver 2017).

A second group of K-mer hits comprised *MprF*, *PgsA*, and multiple *GdpD* homologs, which in other Gram-positive bacteria have been linked to altered membrane phospholipid composition, cell-surface charge, and reduced susceptibility to membrane-active peptide antibiotics, including daptomycin (Yang et al. 2009; Arias et al. 2011; Peleg et al. 2012). In AGA55, these loci most likely represent conserved cell-envelope maintenance functions, but they remain biologically relevant because they may influence susceptibility to cationic antimicrobial peptides and host–microbe interactions. An *RlmA(II)* methyltransferase, annotated as a macrolide/lincosamide target-modifying enzyme, was also detected; however, AGA55's susceptibility to erythromycin and its intermediate sensitivity to azithromycin indicate that this annotation does not translate into an expressed macrolide-resistance phenotype under the conditions tested.

A horizontal gene transfer verification step was applied to assess the safety relevance of the resistome. Protein-BLAST analysis showed that nearly all resistance-associated genes shared 99-100% identity with homologs from *Llb. buchneri* or *Llb. buchneri* subsp. *silagei* (Table S1), indicating that the detected loci are native chromosomal components of the AGA55 lineage rather than recently acquired sequences from taxonomically distant bacteria. Importantly, no well-known transferable resistance determinants, such as acquired *tet* genes, *erm(B)*, chloramphenicol acetyltransferase genes, or complete mobile glycopeptide-resistance operons, were identified, consistent with AGA55's susceptibility to tetracycline and erythromycin. Moreover, two transporter-related hits identified via BV-BRC, namely the Drug

Exporter-2 (DrugE2) Family member Efflux ABC transporter, permease/ATP-binding protein (3.A.1.117.2) and an uncharacterized MFS-type transporter (2. A. 1.2.93), were also detected. However, no data link these systems to a specific acquired-resistance phenotype, so they are therefore interpreted as part of the broader transportome.

The antimicrobial resistance profile of *Llb. buchneri* subsp. *silagei* AGA55 suggests that the detected resistance-associated loci are predominantly conserved chromosomal genes rather than acquired or transferable determinants. The phenotypic results, interpreted according to CLSI guidelines, were consistent with intrinsic resistance patterns commonly reported in lactobacilli, especially reduced susceptibility to aminoglycosides and vancomycin. Genome-based screening further supported this interpretation, as no major mobile resistance determinants, including acquired erythromycin, tetracycline, chloramphenicol acetyltransferase genes, or complete transferable glycopeptide-resistance operons, were detected. Thus, the available phenotypic and genomic data do not indicate a major transferable antimicrobial-resistance risk for AGA55.

Antioxidant Activity and Cholesterol Assimilation

Oxidative stress contributes to cellular damage, chronic inflammation, and the progression of numerous non-communicable diseases, making antioxidant capacity a relevant functional criterion in probiotic evaluation (Feng and Wang 2020; Yetiman et al. 2024). In the present study, the cell-free supernatant (CFS) of *Llb. buchneri* subsp. *silagei* AGA55 demonstrated strong radical-scavenging activity, recording inhibition values of 73.14 ± 0.81% against DPPH and 73.03 ± 0.26% against $ABTS^+$ radicals (Table 6). The near-equivalent activity across the two assays is biologically relevant, since DPPH and $ABTS^+$ differ in their reaction chemistry, solubility conditions, and relative sensitivity to hydrophilic versus lipophilic antioxidants (Prior et al. 2005; Xiao et al. 2025). Therefore, comparable inhibition levels suggest that the effect is not restricted to a single radical system and likely reflects the combined action of multiple secreted reducing agents.

GC–MS analysis of the CFS identified several organic acid derivatives, multiple lactic acid derivatives, xylitol, D-erythronic acid γ-lactone bis(trimethylsilyl) ether, and the non-ribosomally biosynthesized cyclic dipeptide cyclo(L-Pro-L-Leu) (Table 5). Organic acids, hydroxylated metabolites, and cyclic dipeptides produced by lactic acid bacteria have been associated with radical-scavenging activity, reducing capacity, and protection against oxidative damage (Łepecka and Kołożyn-Krajewska 2025; Arslan et al. 2025; Gao et al. 2025). From a genomic perspective, the AGA55 genome encodes a multi-layered oxidative-stress defense repertoire, including thioredoxin/thioredoxin reductase systems, NADH peroxidases, methionine sulfoxide reductases, and metal homeostasis proteins (Table S2), which likely support the intracellular redox environment underlying extracellular antioxidant metabolite secretion (Archibald and Fridovich 1981; Zhao et al. 2010; Lu and Holmgren 2014; Skjoldager et al. 2017; Yetiman et al. 2026). Taken together, the observed DPPH and $ABTS^+$ inhibition values most plausibly reflect the combined extracellular effect of secreted organic acids, polyols, lactic acid derivatives, and the cyclic dipeptide cyclo(L-Pro-L-Leu), rather than a single antioxidant mechanism.

Llb. buchneri subsp. *silage*i AGA55 demonstrated a moderate cholesterol assimilation capacity of 37.04 ± 2.08% (Table 6). This value, while lower than those reported for some well-characterized cholesterol-assimilating lactobacilli

(Pan et al. 2011; Watanabe et al. 2013), confirms a reproducible and quantifiable ability to reduce cholesterol availability in vitro under the tested conditions. The mechanistic basis of cholesterol assimilation in lactobacilli is multifactorial and may involve cell-surface adsorption, co-precipitation with deconjugated bile acids, enzymatic transformation, and incorporation into the cell membrane (Pan et al. 2011; Tomaro-Duchesneau et al. 2014).

Cholesterol oxidase (MetaCyc: PWY-6945; EC 1.1.3.6) is a FAD-dependent flavoenzyme that catalyzes the oxidation of cholesterol to cholest-5-en-3-one, using molecular oxygen as the electron acceptor and generating hydrogen peroxide as a by-product (Kreit and Sampson 2009). The cholesterol dehydrogenase (MetaCyc: PWY-6946) is an $NAD(P)^+$-dependent oxidoreductase that catalyzes a similar overall transformation (cholesterol to cholest-4-en-3-one) but does not require molecular oxygen (Chiang et al. 2008). Importantly, cholesterol oxidase is strictly aerobic, whereas cholesterol dehydrogenase operates via an oxygen-independent mechanism and is therefore better suited to the microaerophilic-to-anaerobic growth conditions characteristic of AGA55 during shalgam fermentation (Chiang et al. 2008; Wang et al. 2013). Consequently, if cholesterol is enzymatically transformed in AGA55, the cholesterol dehydrogenase route is the more physiologically plausible candidate under the fermentation conditions tested. Nevertheless, these assignments are based on automated KEGG/MetaCyc annotations and sequence similarity, and both pathways require experimental verification before definitive conclusions can be drawn.

The mevalonate pathway enzymes, hydroxymethylglutaryl-CoA synthase (PWY-922/K01641/EC:2.3.3.10), hydroxymethylglutaryl-CoA reductase (PWY-5074/ K00054/EC:1.1.1.88), mevalonate kinase (PWY-922/K00869/EC:2.7.1.36), phosphomevalonate kinase (PWY-922/ K00938/ EC:2.7.4.2), diphosphomevalonate decarboxylase (PWY-922/ K01597/EC:4.1.1.33), and acetyl-CoA C-acetyltransferase (K00626/ EC:2.3.1.9), were all detected in the AGA55 genome (Fig. 11, Table S3). In *Lentilactobacillus* and related LAB, this pathway primarily supports the biosynthesis of essential isoprenoid compounds such as undecaprenol (cell-wall lipid carrier), menaquinones (electron transport), and carotenoids, rather than de novo sterol synthesis, which requires downstream enzymatic machinery absent in lactobacilli (Wilding et al. 2000; Kuzuyama and Seto 2012; Bøe and Holo 2020). Nevertheless, membrane lipid composition influences the capacity of bacteria to incorporate exogenous cholesterol into their cell membrane, which is considered one mechanism of cholesterol removal from the growth medium (Tomaro-Duchesneau et al. 2014; Ziarno et al. 2023). Furthermore, a choloylglycine hydrolase (*cbh*) gene was identified in the AGA55 genome, which exhibits bile salt hydrolase-like activity by deconjugating conjugated bile salts into free bile acids (Table S3). These free bile acids co-precipitate with cholesterol at physiological pH, thereby decreasing its micellar solubility and its intestinal absorption (Klaver and van der Meer 1993; Agolino et al. 2024).

In vitro and in silico probiotic examination

The safety, colonization potential, and functional efficacy of a putative probiotic strain are conventionally assessed through a combination of phenotypic assays and genome-based predictions (Hill et al. 2014; Sanders et al. 2019). Accordingly, *Llb. buchneri* subsp. *silagei* AGA55 was evaluated through a comprehensive panel of in vitro probiotic assays, and the phenotypic outcomes were contextualized against genomic features identified through in silico analysis (Table 6).

Hemolytic activity is a primary safety criterion for probiotic candidates, as β-hemolytic strains are excluded from consideration due to the risk of erythrocyte lysis and associated virulence (Kim et al. 2026). AGA55 exhibited γ-hemolysis on sheep blood agar, indicating the complete absence of hemolytic activity. This phenotype is consistent with the in-silico prediction, as genome-wide screening of AGA55 revealed no genes encoding known hemolysins, cytolysin subunits, or related virulence factors.

Autoaggregation capacity reflects the ability of bacterial cells to self-associate, a property linked to intestinal persistence and competitive exclusion of pathogens (Kos et al. 2003; Collado et al. 2008). AGA55 demonstrated a high auto-aggregation rate of 81.60 ± 0.91% (Table 6), which is notably higher than the thresholds reported for established probiotic strains (Haghshenas et al. 2023; Yetiman et al. 2024). At the genomic level, this phenotype is consistent with the presence of genes encoding aggregation-promoting factor (APF), cell wall-anchoring sortase A (*srtA*), and LytR-CpsA-Psr family proteins, which collectively contribute to cell-surface remodeling and intercellular cohesion. Furthermore, genes associated with teichoic acid and lipoteichoic acid biosynthesis, glycosyltransferases, and cell-surface autolysins were identified in the AGA55 genome, collectively supporting a surface architecture conducive to self-aggregation (Table S4).

Cell-surface hydrophobicity, measured by the microbial adhesion to hydrocarbons (MATH) method using xylene, was 28.79 ± 0.88% for AGA55 (Table 6). Although this falls within the moderate hydrophobicity range, it must be interpreted alongside the exceptionally high auto-aggregation capacity, which is a functionally complementary indicator of adhesive fitness, as both parameters collectively govern initial bacterial-epithelial contact and intestinal colonization potential (Collado et al. 2008; Du et al. 2022). Genomic analysis identified multiple lipoproteins, cell-surface hydrolases, and membrane biogenesis-associated proteins that may influence the physicochemical properties of the cell envelope and modulate hydrophobic interactions with host surfaces (Table S4).

Gastrointestinal survival is a prerequisite for a bacterium to exert probiotic effects at the intestinal level. A static in vitro gastrointestinal digestion simulation using the INFOGEST protocol (Brodkorb et al. 2019), as modified by Yetiman (2025), demonstrated that AGA55 maintained substantial viability throughout the simulated digestive process (Table 6). The initial inoculum density was 10.204 log CFU/mL. After 1 h and 2 h of exposure to simulated gastric fluid (SGF; pH 3.0, 2000 U/mL pepsin), the viable counts were 8.544 and 8.359 log CFU/mL, corresponding to survival rates of 83.73% and 81.92%, respectively. Upon transition to simulated intestinal fluid (SIF; pH 7.0, 10 mM bile salts, 100 U/mL pancreatin), viability recovered to 9.498 log CFU/mL (93.08%) at Hour 3 and 9.525 log CFU/mL (93.35%) at Hour 4. This recovery pattern is biologically significant. It suggests that AGA55 cells surviving the gastric phase were metabolically active and proliferative under intestinal conditions. Several genomic features support this robust gastrointestinal resilience. These include Na^+/H^+ antiporters and glutamate decarboxylase-based acid resistance systems, F-type ATPase subunits for proton motive force maintenance, multiple Clp-family proteases (*clpB*, *clpE, clpP, clpX*), *DnaK/DnaJ/GrpE* and *GroES/GroEL* chaperone systems for proteostasis under thermal and acid stress, and general stress response proteins (Table S5-S6). Together, these elements form a multi-layered stress-adaptive system consistent with the high survival rates observed during simulated digestion (van de Guchte et al. 2002; Ljungh and Wadström 2006).

Antimicrobial activity of the cell-free supernatant (CFS) was assessed against five clinically and food-safety-relevant bacterial species using the agar well diffusion method. AGA55 CFS inhibited all tested strains, with inhibition zone diameters ranging from 14.275 ± 0.29 mm (*E. coli* O157:H7 ATCC 43897) to 17.525 ± 0.42 mm (*S. aureus* ATCC 25923) (Table 6). This inhibitory activity against both Gram-positive and Gram-negative strains suggests that the antimicrobial effect is attributable to multiple secreted compounds rather than a single mechanism. The acidic metabolites identified in the GC–MS profile of the CFS, namely lactic acid and its derivatives, acetic acid, and propanoic acid-related compounds (Table 5), likely account for most of the inhibitory activity through pH reduction and direct membrane disruption (Caplice and Fitzgerald 1999; Alakomi et al. 2000). The cyclic dipeptide cyclo(L-Pro-L-Leu) detected in the CFS has also been reported to possess antimicrobial properties, providing an additional bioactive component(Bojarska et al. 2021; Yetiman et al. 2026).

Cytotoxicity versus HT29 and DLD-1 cell lines

The anticancer potential of the cell-free supernatant (CFS) of *Llb. buchneri* subsp. *silagei* AGA55 was evaluated using two human colorectal adenocarcinoma cell lines, HT-29 and DLD-1. These cell lines were selected because they both originate from colorectal cancer, one of the most common malignancies of the gastrointestinal tract, but they differ in their biological characteristics. HT-29 cells are derived from human colon adenocarcinoma and are often used as an intestinal epithelial-like colorectal cancer model. DLD-1 cells are also of human colorectal adenocarcinoma origin, but they represent a more poorly differentiated and genetically unstable cancer phenotype. Therefore, using both cell lines allowed the cytotoxic effect of AGA55-derived metabolites to be examined across two distinct colorectal cancer backgrounds (Yoshida et al. 2011; Ahmed et al. 2013; Martínez-Maqueda et al. 2015).

The CFS of AGA55 reduced the viability of both colorectal cancer cell lines in a concentration-dependent manner. However, the strength of the response differed between HT-29 and DLD-1 cells. In HT-29 cells, low CFS concentrations did not cause evident cytotoxicity. Cell viability remained close to the untreated control at 1 mg/mL and slightly exceeded the control at 2 and 4 mg/mL, with values of 99.97 ± 4.03%, 105.39 ± 3.67%, and 105.04 ± 4.69%, respectively (Fig 9A). A clear inhibitory effect appeared only at higher concentrations. Viability decreased to 63.03 ± 6.31% at 8 mg/mL and further dropped to 13.98 ± 0.82% at 16 mg/mL. Based on dose–response modeling, the IC_{50} value for HT-29 cells was calculated as 8.55 mg/mL (Fig 9B).

DLD-1 cells responded more strongly to the same treatment. Although a slight increase in viability was observed at 1 mg/mL, where viability reached 106.04 ± 1.07%, the inhibitory effect became apparent from 2 mg/mL onward. Cell viability decreased to 90.79 ± 4.04% at 2 mg/mL and then sharply declined to 37.45 ± 1.81% at 4 mg/mL. At 8 mg/mL, viability was reduced to 8.70 ± 0.83%, indicating almost complete suppression of viable cells (Fig 9A). The calculated IC_{50} value for DLD-1 cells was 3.44 mg/mL, which was approximately 2.5 times lower than that observed for HT-29 cells (Fig 9B). This result indicates that DLD-1 cells were substantially more sensitive to AGA55 CFS than HT-29 cells.

The different responses of the two colorectal cancer cell lines may be explained by their distinct cellular phenotypes. HT-29 cells show a more epithelial-like and relatively differentiated colon cancer phenotype, which may provide

greater tolerance against extracellular metabolic stress. In contrast, DLD-1 cells are poorly differentiated and carry molecular features associated with aggressive colorectal cancer behavior. Such cells often display high metabolic demand and altered stress-response pathways. These characteristics may make DLD-1 cells more vulnerable to bacterial metabolites that disturb pH balance, redox homeostasis, mitochondrial function, or energy metabolism(Ahmed et al. 2013; Yetiman et al. 2026).

A mild increase in cell viability at low CFS concentrations was observed in both cell lines, especially in HT-29 cells. This pattern should not necessarily be interpreted as increased cell proliferation. The CCK-8 assay measures cellular metabolic activity, mainly through dehydrogenase-dependent conversion of the tetrazolium reagent (Bouhlel et al. 2026). Therefore, slightly higher absorbance values may reflect transient metabolic stimulation rather than an actual increase in cell number. This biphasic response is consistent with hormesis, where low doses of a biological mixture may stimulate cellular activity, while higher doses become inhibitory or cytotoxic (Calabrese 2008; Mattson 2008). Such behavior is common when cells are exposed to complex fermentation-derived products containing both nutrient-like compounds and inhibitory metabolites.

The cytotoxic effect of AGA55 CFS is likely related to the extracellular metabolites produced by the strain. Lactic acid bacteria can generate several bioactive compounds, including organic acids, short-chain fatty acid-related metabolites, cyclic dipeptides, and other low-molecular-weight molecules with anticancer potential (Rafter 2002; Yetiman et al. 2026). Organic acids may contribute to the observed inhibition by lowering extracellular pH and disrupting intracellular pH regulation. This can interfere with mitochondrial activity, energy production, and cell survival. Cancer cells are particularly sensitive to these disturbances because they depend heavily on altered metabolic pathways to sustain rapid growth.

The GC–MS profile of AGA55 CFS also supports this interpretation. Among the detected compounds, cyclo(L-Pro-L-Leu), a cyclic dipeptide belonging to the diketopiperazine family, is especially relevant. Diketopiperazines are known bioactive molecules with reported cytotoxic, pro-apoptotic, antimicrobial, and signaling-modulatory activities (Vázquez-Rivera et al. 2015). Previous studies have shown that cyclic dipeptides can reduce cancer cell viability by affecting cell-cycle progression, mitochondrial function, oxidative balance, and apoptosis-related pathways (Bojarska et al. 2021). Therefore, cyclo(L-Pro-L-Leu) may be one of the metabolites contributing to the anti-proliferative effect of AGA55 CFS. However, because the CFS was tested as a whole mixture, the role of this compound should be confirmed through fractionation and compound-specific assays.

The present findings are consistent with earlier reports showing that probiotic bacteria and their secreted products can suppress colorectal cancer cell growth. Several studies have linked the anticancer effects of lactic acid bacteria to apoptosis induction, cell-cycle arrest, production of organic acids, modulation of oxidative stress, and regulation of cancer-associated signaling pathways (Liu et al. 2021; Garbacz 2022). Importantly, *Llb. buchneri*-derived membrane vesicles were recently reported to inhibit HT-29 and AGS cancer cells by inducing apoptosis and reducing cell migration (Abedi et al. 2024). This supports the idea that *Llb. buchneri* strains may produce extracellular bioactive components with anticancer relevance.

Carbohydrate-Centered Metabolic Potential of AGA55

Identifying metabolic traits unique to each strain is essential for assessing their potential industrial uses and probiotic benefits (Yetiman et al. 2026). The *Llb. buchneri* sp. *silagei* is a highly adaptable lactic acid bacterium that thrives in diverse environments because it can utilize a wide range of water-soluble carbohydrates (hexose sugars) and, in some cases, organic acids (Heinl et al. 2012; Tanizawa et al. 2020). The API 50 CH assay confirmed that AGA55 has a relatively broad carbohydrate utilization capacity (Fig. 10). The strain fermented 20 of the 49 tested substrates, including common carbohydrates such as D-glucose, D-fructose, D-maltose, D-ribose, and L-arabinose. In addition, AGA55 fermented several plant-associated glycosides, disaccharides, and polyols, including amygdalin, arbutin, D-cellobiose, D-sorbitol, D-trehalose, gentiobiose, salicin, and esculin ferric citrate. These reactions are biologically meaningful because many of these substrates contain β-glucosidic linkages or are associated with vegetable and forage fermentations, where plant cell wall-derived carbohydrates and glycosidic compounds can become available during microbial succession. The positive reactions for D-cellobiose and salicin are especially important, since these substrates were reported as differential traits of *Llb. buchneri* subsp. *silagei* strains SG162^T and NK01 compared with *Llb. buchneri* subsp. *buchneri* reference strains (Tanizawa et al. 2020). Thus, the carbohydrate profile of AGA55 is consistent with its taxonomic assignment and supports its adaptation to plant-derived substrates. Similarly, the ability to ferment D-ribose and L-arabinose indicates that AGA55 can exploit pentose sugars. Pentose utilization is an important feature for strains associated with plant materials because hemicellulose-rich substrates release pentose residues during degradation (Scheller and Ulvskov 2010; Heinl et al. 2012). The positive reaction for N-acetylglucosamine also suggests possible utilization of amino sugar-related substrates, which may originate from microbial cell wall components or complex environmental glycans (Liu et al. 2008; Vollmer et al. 2008).

The strain's capacity to use carbohydrates directly relies on the presence of genes that encode transporters and CAZymes (Yetiman et al. 2026). Most transporters that participate in carbohydrate metabolism are situated within the phosphoenolpyruvate-dependent sugar phosphotransferase system (PTS). The genome of strain AGA55 contains the enzymes related to the phosphotransferase system (PTS). This includes the PTS enzyme I (*ptsI*), the gene for the phosphocarrier protein HPr (*ptsH*, also known as a proton carrier), and other sucrose-, cellobiose-, diacylchitobiose-, and mannose-specific PTS proteins. According to the API50CHL results, there are additional unidentified transporters, or sugar transporters, that may be capable of importing multiple substrates (Kleerebezem et al. 2003). Additionally, the maltose/maltooligosaccharide (PFAM, PF07690) major facilitator superfamily (MFS) transmembrane protein and sn-glycerol 3-phosphate transport system substrate-binding proteins (*ugpBAEC*) were identified in the AGA55 genome.

Heterofermentative species frequently possess the *araBAD* operon, which encodes L-ribulokinase (*araB*), L-arabinose isomerase (*araA*), and L-ribulose-5P-4-epimerase (*araD*). This operon is linked to the catabolism of L-arabinose, a key step in heterofermentation (Buron-Moles et al. 2019). However, two copies of the *araA* gene and one copy of the *araD* gene were detected, whereas the *araB* gene was not detected. Although *araB* was not annotated, the strain fermented L-arabinose in phenotypic assays (Fig 10). This may reflect an alternative or non-canonical catabolic route, functional substitution by an unannotated kinase, or limitations of automated annotation; the duplication of *araA* suggests retained arabinose-isomerase capacity. Targeted analysis would be required to confirm the operative pathway.

Furthermore, the AGA55 genome lacks 1-phosphofructokinase (*pfk*) and fructose-1,6-bisphosphate aldolase; therefore, it cannot utilize hexoses via the EMP pathway. Instead, it processes hexoses through the phosphogluconate pathway, generating not only lactic acid but also substantial amounts of ethanol, acetate, and carbon dioxide (Salvetti et al. 2018; Yetiman et al. 2026). Moreover, it has been confirmed that the enzymes involved in the sequential reaction ending with G-3-P are 6-phosphogluconolactonase (*pgl*), 6-phosphogluconate dehydrogenase (*gntz*), ribulose-phosphate 3-epimerase (*rpe*), and xylulose-5-phosphate/fructose-6-phosphate phosphoketolase (*xpk*) (Heinl et al. 2012). Thus, genome-based metabolic annotation supported these phenotypic findings and revealed that AGA55 has a carbohydrate metabolism typical of obligately heterofermentative lactobacilli (Fig. 11).

The presence of xylose isomerase (*xylA*) and xylulokinase (*xylB*) further suggests that AGA55 can channel pentose sugars into central metabolism. These enzymes convert xylose to xylulose, which is then converted to xylulose-5-phosphate, which can enter the phosphoketolase pathway(Heinl et al. 2012; Yetiman et al. 2026). This genomic prediction aligns with API 50 CH results for pentose-related substrates and supports AGA55's ability to metabolize plant-derived pentose fractions. Similar pentose-utilizing capacity has been reported for *Llb. buchneri* NRRL B-30929, which converted xylose and glucose into lactate, acetate, ethanol, and other products (Liu et al. 2008). Therefore, the carbohydrate metabolism of AGA55 appears consistent with the metabolic flexibility expected from *Llb. buchneri* related strains adapted to plant-rich environments.

Pyruvate metabolism represents a major branch point in AGA55 (Fig. 11). The genome encoded L-lactate dehydrogenase (*ldh*) and D-lactate dehydrogenase (*ldhA*), indicating the potential to produce both lactate isomers. GC–MS analysis supported this prediction by detecting several lactic acid derivatives in the cell-free supernatant (Table 5). Since the samples were derivatized before GC–MS analysis, these compounds were detected as silylated derivatives; however, their repeated detection provides metabolite-level support for active lactic acid fermentation. Lactate production is important because it contributes to acidification, redox balance, and suppression of undesirable microorganisms during fermentation.

In addition to lactate formation, AGA55-encoded enzymes are involved in acetate and ethanol formation, including phosphate acetyltransferase (*pta*) and acetaldehyde/alcohol dehydrogenase (*adhE*). These enzymes are important in heterofermentative metabolism because they link pyruvate-derived carbon flow to the formation of acetyl phosphate, acetate, and ethanol. Acetate-associated metabolism is particularly relevant for *Llb. buchneri* strains because acetic acid contributes to the inhibition of lactate-assimilating yeasts and molds, which are major drivers of heating and aerobic deterioration after silo opening (Oude Elferink et al. 2001; Danner et al. 2003; Drouin et al. 2021). Therefore, the acetate-related enzymatic potential of AGA55 has important functional implications beyond simple carbohydrate utilization.

The silage relevance of AGA55 is further supported by its taxonomic placement within *Llb. buchneri* subsp. *silagei*. This subspecies was originally described from rice grain silage and total mixed ration silage, and later strains have also been recovered from grass silage environments (Heinl et al. 2012; Tanizawa et al. 2020; Irimajiri et al. 2024). In silage systems, *Llb. buchneri* is valued because it can improve aerobic stability by increasing acetic acid formation and reducing yeast growth. The phosphoketolase-centered metabolism, the ability to utilize plant-associated carbohydrates,

and the strain's acetate-related metabolic potential therefore suggest that AGA55 may have silage-relevant potential. However, this conclusion should be interpreted cautiously, because the present data do not include controlled ensiling experiments. Its practical value as a silage inoculant should be confirmed by measuring fermentation profile, pH, lactic acid, acetic acid, propionic acid, ethanol, 1,2-propanediol, yeast and mold counts, dry matter loss, and aerobic stability (Drouin et al. 2021, 2022).

The discrepancies observed between genome-predicted metabolic pathways and GC-MS-detected metabolites highlight the limitations of automated sequence- and orthology-based annotation systems. Although KEGG-BlastKOALA is a robust platform for functional characterization, KO assignment depends on similarity to curated orthologous groups and may fail to resolve divergent, multifunctional, or poorly characterized enzymes, particularly in non-model organisms such as *Llb. buchneri* (Kanehisa et al. 2016). Functional misannotation and overprediction are well-recognized problems in public protein and pathway databases, including automatically annotated resources, especially for enzyme superfamilies containing related proteins with different reaction specificities (Schnoes et al. 2009). More recent experimental-computational analyses have further shown that enzyme-class annotations may require experimental validation because automated assignments can be unreliable for divergent proteins (Rembeza and Engqvist 2021). In the present study, the detection of metabolites and derivatives such as xylitol and D-erythronic acid gamma-lactone in the GC-MS profile provides metabolite-level evidence consistent with metabolic activities that were not fully resolved by genome-based pathway reconstruction. However, because GC-MS identifications were based on spectral library matching after derivatization, these compounds should be interpreted as putatively identified metabolites unless confirmed with authentic standards. Together, the API 50 CH and GC-MS results complement KEGG- and MetaCyc-based genome annotation and provide additional phenotypic and metabolite-level support for AGA55's metabolic versatility. This integrated interpretation is also consistent with the use of multiple pathway databases, since MetaCyc is a literature-curated resource of experimentally elucidated metabolic pathways and enzymes and can provide complementary pathway coverage relative to orthology-based frameworks (Caspi et al. 2016).

Conclusions

This study presents the first genome-resolved multi-omics characterization of *Llb. buchneri* subsp. *silagei* strain AGA55, isolated from traditional Turkish shalgam juice. Taxogenomic analyses using ANI and dDDH unambiguously confirmed the strain's placement within the *Llb. buchneri* subsp. *silagei* clade, while pangenome analysis revealed an open pangenome with substantial genomic plasticity. The bimodal distribution of dDDH values across 27 *Llb. buchneri* genomes further support the existence of at least two distinct genomic subgroups within this species complex. The mobilome of AGA55 is characterized by two PHASTEST-predicted intact prophage-like regions and a diverse IS element repertoire dominated by the IS6 family, collectively indicative of a history of phage- and transposon-mediated genome remodeling. The antimicrobial resistance profile, assessed both phenotypically and genomically, revealed that all detected resistance-associated loci are intrinsic chromosomal features of the *Llb. buchneri* lineage, with no evidence of transferable resistance determinants, supporting the biosafety of this strain. In vitro probiotic screening demonstrated a robust and well-rounded functional profile. AGA55 exhibited high auto-aggregation capacity (81.60%), strong

gastrointestinal survival under simulated digestive conditions, and broad-spectrum antimicrobial activity. Antioxidant assays revealed potent and equivalent radical-scavenging activity against both DPPH and $ABTS^{+}$, which is attributable to the combined action of secreted organic acids, lactic acid derivatives, polyols, and the cyclic dipeptide cyclo(L-Pro-L-Leu). Genomic analysis identified a multi-layered oxidative-stress defense repertoire that likely underpins this extracellular antioxidant capacity. Moderate cholesterol assimilation was observed and supported by genomic evidence for bile salt hydrolase activity, mevalonate pathway enzymes, and membrane lipid-associated mechanisms. The cell-free supernatant of AGA55 also exerted concentration-dependent cytotoxic activity against HT-29 and DLD-1 colorectal adenocarcinoma cell lines, with DLD-1 cells showing greater sensitivity (IC_{50} = 3.44 mg/mL versus 8.55 mg/mL for HT-29), consistent with their poorly differentiated phenotype. Carbohydrate metabolic profiling confirmed the obligately heterofermentative lifestyle of AGA55, with demonstrated capacity to utilize a broad range of plant-associated substrates via the phosphoketolase pathway. The strain's acetate-forming metabolic potential, together with its taxonomic affiliation, further suggests potential utility as a silage inoculant, although this requires dedicated ensiling experiments for validation. Collectively, the integrated genomic, metabolomic, and phenotypic data presented here establish AGA55 as a metabolically versatile and functionally promising candidate with relevance to both food fermentation and probiotic applications. Future studies should focus on in vivo validation of its probiotic efficacy, confirmation of cholesterol transformation pathways through targeted enzymatic assays, and evaluation of its silage-inoculant potential under controlled ensiling conditions.

Funding

The author did not receive any financial support for this study's research and authorship.

Declarations

Conflict of interest

The author declares no competing interests.

References

Abedi A, Tafvizi F, Jafari P, Akbari N (2024) The inhibition effects of Lentilactobacillus buchneri-derived membrane vesicles on AGS and HT-29 cancer cells by inducing cell apoptosis. Sci Rep 14:3100. https://doi.org/10.1038/s41598-024-53773-y

Adejumo IO (2024) Hypothetical proteins of chicken-isolated Limosilactobacillus reuteri subjected to in silico analyses induce IL-2 and IL-10. Genes Nutr 19:21. https://doi.org/10.1186/s12263-024-00755-4

Agolino G, Pino A, Vaccalluzzo A, et al (2024) Bile salt hydrolase: The complexity behind its mechanism in relation to lowering-cholesterol lactobacilli probiotics. Journal of Functional Foods 120:106357. https://doi.org/10.1016/j.jff.2024.106357

Ahmed D, Eide PW, Eilertsen IA, et al (2013) Epigenetic and genetic features of 24 colon cancer cell lines. Oncogenesis 2:e71–e71. https://doi.org/10.1038/oncsis.2013.35

Alakomi H-L, Skyttä E, Saarela M, et al (2000) Lactic Acid Permeabilizes Gram-Negative Bacteria by Disrupting the Outer Membrane. Applied and Environmental Microbiology 66:2001–2005. https://doi.org/10.1128/AEM.66.5.2001-2005.2000

Alcock BP, Raphenya AR, Lau TTY, et al (2020) CARD 2020: antibiotic resistome surveillance with the comprehensive antibiotic resistance database. Nucleic Acids Res 48:D517–D525. https://doi.org/10.1093/nar/gkz935

Alikhan N-F, Petty NK, Ben Zakour NL, Beatson SA (2011) BLAST Ring Image Generator (BRIG): simple prokaryote genome comparisons. BMC Genomics 12:402. https://doi.org/10.1186/1471-2164-12-402

Ammor MS, Belén Flórez A, Mayo B (2007) Antibiotic resistance in non-enterococcal lactic acid bacteria and bifidobacteria. Food Microbiology 24:559–570. https://doi.org/10.1016/j.fm.2006.11.001

Archibald FS, Fridovich I (1981) Manganese and Defenses against Oxygen Toxicity in Lactobacillus plantarum. Journal of Bacteriology 145:442–451. https://doi.org/10.1128/jb.145.1.442-451.1981

Arias CA, Panesso D, McGrath DM, et al (2011) Genetic Basis for In Vivo Daptomycin Resistance in Enterococci. New England Journal of Medicine 365:892–900. https://doi.org/10.1056/NEJMoa1011138

Arndt D, Grant JR, Marcu A, et al (2016a) PHASTER: a better, faster version of the PHAST phage search tool. Nucleic Acids Res 44:W16-21. https://doi.org/10.1093/nar/gkw387

Arndt D, Grant JR, Marcu A, et al (2016b) PHASTER: a better, faster version of the PHAST phage search tool. Nucleic Acids Res 44:W16-21. https://doi.org/10.1093/nar/gkw387

Arslan NP, Azad F, Orak T, et al (2025) A review on bacteria-derived antioxidant metabolites: their production, purification, characterization, potential applications, and limitations. Arch Pharm Res 48:253–292. https://doi.org/10.1007/s12272-025-01541-5

Blair JMA, Webber MA, Baylay AJ, et al (2015) Molecular mechanisms of antibiotic resistance. Nat Rev Microbiol 13:42–51. https://doi.org/10.1038/nrmicro3380

Bøe CA, Holo H (2020) Engineering Lactococcus lactis for Increased Vitamin K2 Production. Front Bioeng Biotechnol 8:. https://doi.org/10.3389/fbioe.2020.00191

Bojarska J, Mieczkowski A, Ziora ZM, et al (2021) Cyclic Dipeptides: The Biological and Structural Landscape with Special Focus on the Anti-Cancer Proline-Based Scaffold. Biomolecules 11:1515. https://doi.org/10.3390/biom11101515

Bonacina J, Suárez N, Hormigo R, et al (2017) A genomic view of food-related and probiotic Enterococcus strains. DNA Res 24:11–24. https://doi.org/10.1093/dnares/dsw043

Borowska M, Buttimer C, Bottacini F, et al (2025) Comparative genomic analysis of selected lactic acid bacteria and phenotypic association of the key genes involved in fructan and ribose utilisation. Discov Bact 2:5. https://doi.org/10.1007/s44351-025-00016-8

Bouhlel W, Doğan M, Yetiman AE, et al (2026) Investigation of the Microbiocidal, Antioxidant, and Cytotoxic Effects of Cinnamomum verum (Cinnamon), Origanum onites (Oregano Balls), and Origanum vulgare (Black Oregano) Hydrosols: A Model Food Environment-Driven Usability Study. Food Bioprocess Technol 19:166. https://doi.org/10.1007/s11947-026-04258-5

Brettin T, Davis JJ, Disz T, et al (2015) RASTtk: A modular and extensible implementation of the RAST algorithm for building custom annotation pipelines and annotating batches of genomes. Sci Rep 5:8365. https://doi.org/10.1038/srep08365

Brodkorb A, Egger L, Alminger M, et al (2019) INFOGEST static in vitro simulation of gastrointestinal food digestion. Nat Protoc 14:991–1014. https://doi.org/10.1038/s41596-018-0119-1

Buron-Moles G, Chailyan A, Dolejs I, et al (2019) Uncovering carbohydrate metabolism through a genotype-phenotype association study of 56 lactic acid bacteria genomes. Appl Microbiol Biotechnol 103:3135–3152. https://doi.org/10.1007/s00253-019-09701-6

Calabrese EJ (2008) Hormesis and medicine. British Journal of Clinical Pharmacology 66:594–617. https://doi.org/10.1111/j.1365-2125.2008.03243.x

Campbell EA, Korzheva N, Mustaev A, et al (2001) Structural Mechanism for Rifampicin Inhibition of Bacterial RNA Polymerase. Cell 104:901–912. https://doi.org/10.1016/S0092-8674(01)00286-0

Canchaya C, Fournous G, Brüssow H (2004) The impact of prophages on bacterial chromosomes. Mol Microbiol 53:9–18. https://doi.org/10.1111/j.1365-2958.2004.04113.x

Caplice E, Fitzgerald GF (1999) Food fermentations: role of microorganisms in food production and preservation. Int J Food Microbiol 50:131–149. https://doi.org/10.1016/s0168-1605(99)00082-3

Casjens S (2003) Prophages and bacterial genomics: what have we learned so far? Mol Microbiol 49:277–300. https://doi.org/10.1046/j.1365-2958.2003.03580.x

Caspi R, Billington R, Ferrer L, et al (2016) The MetaCyc database of metabolic pathways and enzymes and the BioCyc collection of pathway/genome databases. Nucleic Acids Res 44:D471-480. https://doi.org/10.1093/nar/gkv1164

Chen I-MA, Chu K, Palaniappan K, et al (2023) The IMG/M data management and analysis system v.7: content updates and new features. Nucleic Acids Res 51:D723–D732. https://doi.org/10.1093/nar/gkac976

Chiang Y-R, Ismail W, Heintz D, et al (2008) Study of Anoxic and Oxic Cholesterol Metabolism by Sterolibacterium denitrificans. J Bacteriol 190:905–914. https://doi.org/10.1128/JB.01525-07

CLSI (2023) Performance Standards for Antimicrobial Susceptibility Testing. Clinical and Laboratory Standards Institute, Wayne, PA

Collado MC, Meriluoto J, Salminen S (2008) Adhesion and aggregation properties of probiotic and pathogen strains. Eur Food Res Technol 226:1065–1073. https://doi.org/10.1007/s00217-007-0632-x

Courvalin P (2006) Vancomycin Resistance in Gram-Positive Cocci. Clin Infect Dis 42:S25–S34. https://doi.org/10.1086/491711

Danner H, Holzer M, Mayrhuber E, Braun R (2003) Acetic Acid Increases Stability of Silage under Aerobic Conditions. Applied and Environmental Microbiology 69:562–567. https://doi.org/10.1128/AEM.69.1.562-567.2003

Davis JJ, Boisvert S, Brettin T, et al (2016) Antimicrobial Resistance Prediction in PATRIC and RAST. Sci Rep 6:27930. https://doi.org/10.1038/srep27930

Dereeper A, Summo M, Meyer DF (2022) PanExplorer: a web-based tool for exploratory analysis and visualization of bacterial pan-genomes. Bioinformatics 38:4412–4414. https://doi.org/10.1093/bioinformatics/btac504

Douillard FP, de Vos WM (2014) Functional genomics of lactic acid bacteria: from food to health. Microb Cell Fact 13:S8. https://doi.org/10.1186/1475-2859-13-S1-S8

Drouin P, Tremblay J, da Silva ÉB, Apper E (2022) Changes to the microbiome of alfalfa during the growing season and after ensiling with Lentilactobacillus buchneri and Lentilactobacillus hilgardii inoculant. J Appl Microbiol 133:2331–2347. https://doi.org/10.1111/jam.15641

834 Drouin P, Tremblay J, Renaud J, Apper E (2021) Microbiota succession during aerobic stability of maize silage
835 inoculated with Lentilactobacillus buchneri NCIMB 40788 and Lentilactobacillus hilgardii CNCM-I-4785.
836 Microbiologyopen 10:e1153. https://doi.org/10.1002/mbo3.1153

837 Du Y, Li H, Shao J, et al (2022) Adhesion and Colonization of the Probiotic Lactobacillus plantarum HC-2 in the
838 Intestine of Litopenaeus Vannamei Are Associated With Bacterial Surface Proteins. Front Microbiol
839 13:878874. https://doi.org/10.3389/fmicb.2022.878874

840 Duar RM, Lin XB, Zheng J, et al (2017) Lifestyles in transition: evolution and natural history of the genus
841 Lactobacillus. FEMS Microbiol Rev 41:S27–S48. https://doi.org/10.1093/femsre/fux030

842 EFSA-FEEDAP (2012) Guidance on the assessment of bacterial susceptibility to antimicrobials of human and
843 veterinary importance. EFSA Journal 10:2740. https://doi.org/10.2903/j.efsa.2012.2740

844 Ekinci FY, Baser GM, Özcan E, et al (2016) Characterization of chemical, biological, and antiproliferative properties
845 of fermented black carrot juice, shalgam. Eur Food Res Technol 242:1355–1368.
846 https://doi.org/10.1007/s00217-016-2639-7

847 Feng T, Wang J (2020) Oxidative stress tolerance and antioxidant capacity of lactic acid bacteria as probiotic: a
848 systematic review. Gut Microbes 12:1801944. https://doi.org/10.1080/19490976.2020.1801944

849 Fouts DE (2006) Phage_Finder: automated identification and classification of prophage regions in complete bacterial
850 genome sequences. Nucleic Acids Res 34:5839–5851. https://doi.org/10.1093/nar/gkl732

851 Gao Y, Liang Q, Sun J, et al (2025) Probiotic potential of lactic acid bacteria with antioxidant properties in
852 modulating health: Mechanisms, applications, and future directions. Food Bioscience 66:106181.
853 https://doi.org/10.1016/j.fbio.2025.106181

854 Garbacz K (2022) Anticancer activity of lactic acid bacteria. Seminars in Cancer Biology 86:356–366.
855 https://doi.org/10.1016/j.semcancer.2021.12.013

856 Goldstein EJC, Tyrrell KL, Citron DM (2015) Lactobacillus Species: Taxonomic Complexity and Controversial
857 Susceptibilities. Clin Infect Dis 60:S98–S107. https://doi.org/10.1093/cid/civ072

858 Haghshenas B, Kiani A, Mansoori S, et al (2023) Probiotic properties and antimicrobial evaluation of silymarin-
859 enriched Lactobacillus bacteria isolated from traditional curd. Sci Rep 13:10916.
860 https://doi.org/10.1038/s41598-023-37350-3

861 Heinl S, Grabherr R (2017) Systems biology of robustness and flexibility: *Lactobacillus buchneri*—A show case.
862 Journal of Biotechnology 257:61–69. https://doi.org/10.1016/j.jbiotec.2017.01.007

863 Heinl S, Wibberg D, Eikmeyer F, et al (2012) Insights into the completely annotated genome of Lactobacillus
864 buchneri CD034, a strain isolated from stable grass silage. J Biotechnol 161:153–166.
865 https://doi.org/10.1016/j.jbiotec.2012.03.007

866 Hill C, Guarner F, Reid G, et al (2014) The International Scientific Association for Probiotics and Prebiotics
867 consensus statement on the scope and appropriate use of the term probiotic. Nat Rev Gastroenterol Hepatol
868 11:506–514. https://doi.org/10.1038/nrgastro.2014.66

869 Hooper DC, Jacoby GA (2015) Mechanisms of drug resistance: quinolone resistance. Annals of the New York
870 Academy of Sciences 1354:12–31. https://doi.org/10.1111/nyas.12830

871 Huerta-Cepas J, Forslund K, Coelho LP, et al (2017) Fast Genome-Wide Functional Annotation through Orthology
872 Assignment by eggNOG-Mapper. Mol Biol Evol 34:2115–2122. https://doi.org/10.1093/molbev/msx148

873 Huerta-Cepas J, Szklarczyk D, Heller D, et al (2019) eggNOG 5.0: a hierarchical, functionally and phylogenetically
874 annotated orthology resource based on 5090 organisms and 2502 viruses. Nucleic Acids Res 47:D309–
875 D314. https://doi.org/10.1093/nar/gky1085

876 Irimajiri R, Kuwabara M, Togo S, et al (2024) Complete genome sequence of Lentilactobacillus buchneri subsp.
877 silagei MGR2-32 isolated from guinea grass silage in Okinawa, Japan. Microbiol Resour Announc
878 13:e0069523. https://doi.org/10.1128/mra.00695-23

879 Jain C, Rodriguez-R LM, Phillippy AM, et al (2018) High throughput ANI analysis of 90K prokaryotic genomes
880 reveals clear species boundaries. Nat Commun 9:5114. https://doi.org/10.1038/s41467-018-07641-9

881 Jarocki P, Komoń-Janczara E, Młodzińska A, et al (2023) Occurrence and genetic diversity of prophage sequences
882 identified in the genomes of L. casei group bacteria. Sci Rep 13:8603. https://doi.org/10.1038/s41598-023-
883 35823-z

884 Juhas M, van der Meer JR, Gaillard M, et al (2009) Genomic islands: tools of bacterial horizontal gene transfer and
885 evolution. FEMS Microbiol Rev 33:376–393. https://doi.org/10.1111/j.1574-6976.2008.00136.x

886 Kanehisa M, Sato Y, Morishima K (2016) BlastKOALA and GhostKOALA: KEGG Tools for Functional
887 Characterization of Genome and Metagenome Sequences. J Mol Biol 428:726–731.
888 https://doi.org/10.1016/j.jmb.2015.11.006

889 Karaman MZ, Yetiman AE, Zhan J, Fidan O (2025) Biochemical Characterization and Genome Analysis of
890 Pseudomonas loganensis sp. nov., a Novel Endophytic Bacterium. MicrobiologyOpen 14:e70051.
891 https://doi.org/10.1002/mbo3.70051

892 Khan ZA, Siddiqui MF, Park S (2019) Current and Emerging Methods of Antibiotic Susceptibility Testing.
893 Diagnostics (Basel) 9:49. https://doi.org/10.3390/diagnostics9020049

894 Kim H, Lee HH, Song S, et al (2026) Genome-Informed Characterization of Lactiplantibacillus plantarum ND88
895 with Inhibitory Activity against Representative Oral Pathogens. Probiotics & Antimicro Prot.
896 https://doi.org/10.1007/s12602-026-10992-1

897 Klaver FA, van der Meer R (1993) The assumed assimilation of cholesterol by Lactobacilli and Bifidobacterium
898 bifidum is due to their bile salt-deconjugating activity. Applied and Environmental Microbiology 59:1120–
899 1124. https://doi.org/10.1128/aem.59.4.1120-1124.1993

900 Kleerebezem M, Boekhorst J, van Kranenburg R, et al (2003) Complete genome sequence of Lactobacillus
901 plantarum WCFS1. Proceedings of the National Academy of Sciences 100:1990–1995.
902 https://doi.org/10.1073/pnas.0337704100

903 Kos B, Šušković J, Vuković S, et al (2003) Adhesion and aggregation ability of probiotic strain Lactobacillus
904 acidophilus M92. J Appl Microbiol 94:981–987. https://doi.org/10.1046/j.1365-2672.2003.01915.x

905 Krause KM, Serio AW, Kane TR, Connolly LE (2016) Aminoglycosides: An Overview. Cold Spring Harb Perspect
906 Med 6:a027029. https://doi.org/10.1101/cshperspect.a027029

907 Kreit J, Sampson NS (2009) Cholesterol oxidase: physiological functions. FEBS J 276:6844–6856.
908 https://doi.org/10.1111/j.1742-4658.2009.07378.x

909 Kutmon M, Van Iersel MP, Bohler A, et al (2015) PathVisio 3: An Extendable Pathway Analysis Toolbox. PLoS
910 Comput Biol 11:e1004085. https://doi.org/10.1371/journal.pcbi.1004085

911 Kuzuyama T, Seto H (2012) Two distinct pathways for essential metabolic precursors for isoprenoid biosynthesis.
912 Proceedings of the Japan Academy, Series B 88:41–52. https://doi.org/10.2183/pjab.88.41

Langille MGI, Hsiao WWL, Brinkman FSL (2010) Detecting genomic islands using bioinformatics approaches. Nat Rev Microbiol 8:373–382. https://doi.org/10.1038/nrmicro2350

Łepecka A, Kołożyn-Krajewska D (2025) Antioxidant Properties of Food-Derived Lactic Acid Bacteria: A Review. Microbial Biotechnology 18:e70229. https://doi.org/10.1111/1751-7915.70229

Liu C, Zheng J, Ou X, Han Y (2021) Anti-cancer Substances and Safety of Lactic Acid Bacteria in Clinical Treatment. Front Microbiol 12:. https://doi.org/10.3389/fmicb.2021.722052

Liu Q, Guo X, Zhang J, et al (2026) An integrated genomic and phenotypic analysis insight into the comprehensive safety assessment of the potential probiotic *Lactiplantibacillus plantarum* TSP05. Food Bioscience 79:108858. https://doi.org/10.1016/j.fbio.2026.108858

Liu S, Leathers TD, Copeland A, et al (2011) Complete Genome Sequence of Lactobacillus buchneri NRRL B-30929, a Novel Strain from a Commercial Ethanol Plant. J Bacteriol 193:4019–4020. https://doi.org/10.1128/JB.05180-11

Liu S, Skinner-Nemec KA, Leathers TD (2008) Lactobacillus buchneri strain NRRL B-30929 converts a concentrated mixture of xylose and glucose into ethanol and other products. J Ind Microbiol Biotechnol 35:75–81. https://doi.org/10.1007/s10295-007-0267-8

Ljungh A, Wadström T (2006) Lactic acid bacteria as probiotics. Curr Issues Intest Microbiol 7:73–89

Lu J, Holmgren A (2014) The thioredoxin antioxidant system. Free Radical Biology and Medicine 66:75–87. https://doi.org/10.1016/j.freeradbiomed.2013.07.036

Mahillon J, Chandler M (1998) Insertion sequences. Microbiol Mol Biol Rev 62:725–774. https://doi.org/10.1128/MMBR.62.3.725-774.1998

Maione A, Imparato M, Buonanno A, et al (2024) Evaluation of Potential Probiotic Properties and In Vivo Safety of Lactic Acid Bacteria and Yeast Strains Isolated from Traditional Home-Made Kefir. Foods 13:1013. https://doi.org/10.3390/foods13071013

Makarova K, Slesarev A, Wolf Y, et al (2006) Comparative genomics of the lactic acid bacteria. Proc Natl Acad Sci U S A 103:15611–15616. https://doi.org/10.1073/pnas.0607117103

Marshall CG, Broadhead G, Leskiw BK, Wright GD (1997) d-Ala-d-Ala ligases from glycopeptide antibiotic-producing organisms are highly homologous to the enterococcal vancomycin-resistance ligases VanA and VanB. Proceedings of the National Academy of Sciences 94:6480–6483. https://doi.org/10.1073/pnas.94.12.6480

Martínez-Maqueda D, Miralles B, Recio I (2015) HT29 Cell Line. In: Verhoeckx K, Cotter P, López-Expósito I, et al. (eds) The Impact of Food Bioactives on Health: in vitro and ex vivo models. Springer International Publishing, Cham, pp 113–124

Mattson MP (2008) Hormesis defined. Ageing Research Reviews 7:1–7. https://doi.org/10.1016/j.arr.2007.08.007

Meier-Kolthoff JP, Auch AF, Klenk H-P, Göker M (2013) Genome sequence-based species delimitation with confidence intervals and improved distance functions. BMC Bioinformatics 14:60. https://doi.org/10.1186/1471-2105-14-60

Meier-Kolthoff JP, Carbasse JS, Peinado-Olarte RL, Göker M (2022) TYGS and LPSN: a database tandem for fast and reliable genome-based classification and nomenclature of prokaryotes. Nucleic Acids Res 50:D801–D807. https://doi.org/10.1093/nar/gkab902

Merrick CA, Zhao J, Rosser SJ (2018) Serine Integrases: Advancing Synthetic Biology. ACS Synth Biol 7:299–310. https://doi.org/10.1021/acssynbio.7b00308

Mosquera-Rendón J, Rada-Bravo AM, Cárdenas-Brito S, et al (2016) Pangenome-wide and molecular evolution analyses of the Pseudomonas aeruginosa species. BMC Genomics 17:45. https://doi.org/10.1186/s12864-016-2364-4

Nethery MA, Henriksen ED, Daughtry KV, et al (2019) Comparative genomics of eight Lactobacillus buchneri strains isolated from food spoilage. BMC Genomics 20:902. https://doi.org/10.1186/s12864-019-6274-0

Olson RD, Assaf R, Brettin T, et al (2023) Introducing the Bacterial and Viral Bioinformatics Resource Center (BV-BRC): a resource combining PATRIC, IRD and ViPR. Nucleic Acids Res 51:D678–D689. https://doi.org/10.1093/nar/gkac1003

Oude Elferink SJWH, Krooneman J, Gottschal JC, et al (2001) Anaerobic Conversion of Lactic Acid to Acetic Acid and 1,2-Propanediol by Lactobacillus buchneri. Applied and Environmental Microbiology 67:125–132. https://doi.org/10.1128/AEM.67.1.125-132.2001

Pan DD, Zeng XQ, Yan YT (2011) Characterisation of Lactobacillus fermentum SM-7 isolated from koumiss, a potential probiotic bacterium with cholesterol-lowering effects. J Sci Food Agric 91:512–518. https://doi.org/10.1002/jsfa.4214

Peleg AY, Miyakis S, Ward DV, et al (2012) Whole Genome Characterization of the Mechanisms of Daptomycin Resistance in Clinical and Laboratory Derived Isolates of Staphylococcus aureus. PLOS ONE 7:e28316. https://doi.org/10.1371/journal.pone.0028316

Perrin A, Rocha EPC (2021) PanACoTA: a modular tool for massive microbial comparative genomics. NAR Genom Bioinform 3:lqaa106. https://doi.org/10.1093/nargab/lqaa106

Prior RL, Wu X, Schaich K (2005) Standardized Methods for the Determination of Antioxidant Capacity and Phenolics in Foods and Dietary Supplements. J Agric Food Chem 53:4290–4302. https://doi.org/10.1021/jf0502698

R Core Team (2024) R: A Language and Environment for Statistical Computing

Rafter J (2002) Lactic acid bacteria and cancer: mechanistic perspective. British Journal of Nutrition 88:S89–S94. https://doi.org/10.1079/BJN2002633

Raya RR, Fremaux C, De Antoni GL, Klaenhammer TR (1992) Site-specific integration of the temperate bacteriophage phi adh into the Lactobacillus gasseri chromosome and molecular characterization of the phage (attP) and bacterial (attB) attachment sites. J Bacteriol 174:5584–5592. https://doi.org/10.1128/jb.174.17.5584-5592.1992

Reimer LC, Vetcininova A, Carbasse JS, et al (2019) BacDive in 2019: bacterial phenotypic data for High-throughput biodiversity analysis. Nucleic Acids Res 47:D631–D636. https://doi.org/10.1093/nar/gky879

Rembeza E, Engqvist MKM (2021) Experimental and computational investigation of enzyme functional annotations uncovers misannotation in the EC 1.1.3.15 enzyme class. PLOS Computational Biology 17:e1009446. https://doi.org/10.1371/journal.pcbi.1009446

Reynolds PE (1989) Structure, biochemistry and mechanism of action of glycopeptide antibiotics. Eur J Clin Microbiol Infect Dis 8:943–950. https://doi.org/10.1007/BF01967563

Richter M, Rosselló-Móra R (2009) Shifting the genomic gold standard for the prokaryotic species definition. Proceedings of the National Academy of Sciences 106:19126–19131. https://doi.org/10.1073/pnas.0906412106

Rodriguez-R LM, Conrad RE, Viver T, et al (2023) An ANI gap within bacterial species that advances the definitions of intra-species units. mBio 15:e02696-23. https://doi.org/10.1128/mbio.02696-23

Salvetti E, Harris HMB, Felis GE, O'Toole PW (2018) Comparative Genomics of the Genus Lactobacillus Reveals Robust Phylogroups That Provide the Basis for Reclassification. Applied and Environmental Microbiology 84:e00993-18. https://doi.org/10.1128/AEM.00993-18

Sanders ME, Merenstein DJ, Reid G, et al (2019) Probiotics and prebiotics in intestinal health and disease: from biology to the clinic. Nat Rev Gastroenterol Hepatol 16:605–616. https://doi.org/10.1038/s41575-019-0173-3

Scheller HV, Ulvskov P (2010) Hemicelluloses. Annual Review of Plant Biology 61:263–289. https://doi.org/10.1146/annurev-arplant-042809-112315

Schnoes AM, Brown SD, Dodevski I, Babbitt PC (2009) Annotation error in public databases: misannotation of molecular function in enzyme superfamilies. PLoS Comput Biol 5:e1000605. https://doi.org/10.1371/journal.pcbi.1000605

Seemann T (2014) Prokka: rapid prokaryotic genome annotation. Bioinformatics 30:2068–2069. https://doi.org/10.1093/bioinformatics/btu153

Siguier P, Gourbeyre E, Chandler M (2014) Bacterial insertion sequences: their genomic impact and diversity. FEMS Microbiol Rev 38:865–891. https://doi.org/10.1111/1574-6976.12067

Silver LL (2017) Fosfomycin: Mechanism and Resistance. Cold Spring Harb Perspect Med 7:a025262. https://doi.org/10.1101/cshperspect.a025262

Skjoldager N, Blanner Bang M, Rykær M, et al (2017) The structure of Lactococcus lactis thioredoxin reductase reveals molecular features of photo-oxidative damage. Sci Rep 7:46282. https://doi.org/10.1038/srep46282

Sköld O (2001) Resistance to trimethoprim and sulfonamides. Vet Res 32:261–273. https://doi.org/10.1051/vetres:2001123

Tanizawa Y, Kobayashi H, Nomura M, et al (2020) Lactobacillus buchneri subsp. silagei subsp. nov., isolated from rice grain silage. Int J Syst Evol Microbiol 70:3111–3116. https://doi.org/10.1099/ijsem.0.004138

Tatusov RL, Fedorova ND, Jackson JD, et al (2003) The COG database: an updated version includes eukaryotes. BMC Bioinformatics 4:41. https://doi.org/10.1186/1471-2105-4-41

Tatusova T, DiCuccio M, Badretdin A, et al (2016) NCBI prokaryotic genome annotation pipeline. Nucleic Acids Res 44:6614–6624. https://doi.org/10.1093/nar/gkw569

Tettelin H, Masignani V, Cieslewicz MJ, et al (2005) Genome analysis of multiple pathogenic isolates of *Streptococcus agalactiae* : Implications for the microbial "pan-genome." Proc Natl Acad Sci USA 102:13950–13955. https://doi.org/10.1073/pnas.0506758102

Tettelin H, Riley D, Cattuto C, Medini D (2008) Comparative genomics: the bacterial pan-genome. Current Opinion in Microbiology 11:472–477. https://doi.org/10.1016/j.mib.2008.09.006

Tomaro-Duchesneau C, Jones ML, Shah D, et al (2014) Cholesterol Assimilation by *Lactobacillus* Probiotic Bacteria: An *In Vitro* Investigation. BioMed Research International 2014:1–9. https://doi.org/10.1155/2014/380316

Vale FF, Nunes A, Oleastro M, et al (2017) Genomic structure and insertion sites of Helicobacter pylori prophages from various geographical origins. Sci Rep 7:42471. https://doi.org/10.1038/srep42471

van de Guchte M, Serror P, Chervaux C, et al (2002) Stress responses in lactic acid bacteria. Antonie Van Leeuwenhoek 82:187–216. https://doi.org/10.1023/A:1020631532202

Vandecraen J, Chandler M, Aertsen A, Van Houdt R (2017) The impact of insertion sequences on bacterial genome plasticity and adaptability. Crit Rev Microbiol 43:709–730. https://doi.org/10.1080/1040841X.2017.1303661

Vázquez-Rivera D, González O, Guzmán-Rodríguez J, et al (2015) Cytotoxicity of Cyclodipeptides from Pseudomonas aeruginosa PAO1 Leads to Apoptosis in Human Cancer Cell Lines. BioMed Research International 2015:197608. https://doi.org/10.1155/2015/197608

Vollmer W, Blanot D, De Pedro MA (2008) Peptidoglycan structure and architecture. FEMS Microbiol Rev 32:149–167. https://doi.org/10.1111/j.1574-6976.2007.00094.x

Wang P-H, Lee T-H, Ismail W, et al (2013) An Oxygenase-Independent Cholesterol Catabolic Pathway Operates under Oxic Conditions. PLOS ONE 8:e66675. https://doi.org/10.1371/journal.pone.0066675

Watanabe S, Katsube T, Hattori H, et al (2013) Effect of *Lactobacillus brevis* 119-2 isolated from Tsuda kabu red turnips on cholesterol levels in cholesterol-administered rats. Journal of Bioscience and Bioengineering 116:45–51. https://doi.org/10.1016/j.jbiosc.2013.01.009

Wilding EI, Brown JR, Bryant AP, et al (2000) Identification, Evolution, and Essentiality of the Mevalonate Pathway for Isopentenyl Diphosphate Biosynthesis in Gram-Positive Cocci. Journal of Bacteriology 182:4319–4327. https://doi.org/10.1128/jb.182.15.4319-4327.2000

Wishart DS, Han S, Saha S, et al (2023) PHASTEST: faster than PHASTER, better than PHAST. Nucleic Acids Res 51:W443–W450. https://doi.org/10.1093/nar/gkad382

Xiao Y, Yang J, Zhang X, et al (2025) Evaluation and mechanism of the antioxidant activity of lactic acid bacteria. Folia Microbiol 70:711–727. https://doi.org/10.1007/s12223-025-01277-1

Yang S-J, Xiong YQ, Dunman PM, et al (2009) Regulation of mprF in Daptomycin-Nonsusceptible Staphylococcus aureus Strains. Antimicrobial Agents and Chemotherapy 53:2636–2637. https://doi.org/10.1128/aac.01415-08

Yetiman A (2025) Pangenome analysis and “in silico” overview of carbohydrate and vitamin metabolism of Lactiplantibacillus plantarum strain TRA56 obtained from lactic-acid fermented beverage known as Shalgam. Biotech Studies 34:1–17. https://doi.org/10.38042/biotechstudies.1615601

Yetiman A, Horzum M, Bahar D, Akbulut M (2024) Assessment of Genomic and Metabolic Characteristics of Cholesterol-Reducing and GABA Producer Limosilactobacillus fermentum AGA52 Isolated from Lactic Acid Fermented Shalgam Based on “In Silico” and “In Vitro” Approaches. Probiotics & Antimicro Prot 16:334–351. https://doi.org/10.1007/s12602-022-10038-2

Yetiman AE, Horzum M, Kanbur E, et al (2026) Pangenome Analysis and Genome-Guided Probiotic Evaluation of Cyclic Dipeptides Producing Levilactobacillus brevis DY55bre Strain from a Lactic Acid Fermented Shalgam to Assess Its Metabolic, Probiotic Potentials, and Cytotoxic Effects on Colorectal Cancer Cells. Probiotics & Antimicro Prot 18:4540–4568. https://doi.org/10.1007/s12602-025-10760-7

Yetiman AE, Horzum M, Kanbur E, et al (2025) Pangenome Analysis and Genome-Guided Probiotic Evaluation of Cyclic Dipeptides Producing Levilactobacillus brevis DY55bre Strain from a Lactic Acid Fermented Shalgam to Assess Its Metabolic, Probiotic Potentials, and Cytotoxic Effects on Colorectal Cancer Cells. Probiotics & Antimicro Prot. https://doi.org/10.1007/s12602-025-10760-7

Yetiman AE, Keskin A, Darendeli BN, et al (2022) Characterization of genomic, physiological, and probiotic features *Lactiplantibacillus plantarum* DY46 strain isolated from traditional lactic acid fermented shalgam beverage. Food Bioscience 46:101499. https://doi.org/10.1016/j.fbio.2021.101499

Yoshida R, Miyashita K, Inoue M, et al (2011) Concurrent genetic alterations in DNA polymerase proofreading and mismatch repair in human colorectal cancer. Eur J Hum Genet 19:320–325. https://doi.org/10.1038/ejhg.2010.216

Zhai Y, Wei C (2022) Open pangenome of Lactococcus lactis generated by a combination of metagenome-assembled genomes and isolate genomes. Front Microbiol 13:948138. https://doi.org/10.3389/fmicb.2022.948138

Zhao C, Hartke A, La Sorda M, et al (2010) Role of Methionine Sulfoxide Reductases A and B of Enterococcus faecalis in Oxidative Stress and Virulence. Infection and Immunity 78:3889–3897. https://doi.org/10.1128/iai.00165-10

Zheng J, Ge Q, Yan Y, et al (2023) dbCAN3: automated carbohydrate-active enzyme and substrate annotation. Nucleic Acids Res 51:W115–W121. https://doi.org/10.1093/nar/gkad328

Zheng J, Wittouck S, Salvetti E, et al (2020) A taxonomic note on the genus Lactobacillus: Description of 23 novel genera, emended description of the genus Lactobacillus Beijerinck 1901, and union of Lactobacillaceae and Leuconostocaceae. International Journal of Systematic and Evolutionary Microbiology 70:2782–2858. https://doi.org/10.1099/ijsem.0.004107

Ziarno M, Zaręba D, Ścibisz I, Kozłowska M (2023) Exploring the Cholesterol-Modifying Abilities of Lactobacilli Cells in Digestive Models and Dairy Products. Microorganisms 11:1478. https://doi.org/10.3390/microorganisms11061478

Table 1. Descriptive statistics of the *Llb. buchneri* sp. *silagei* AGA55 genome based on best-placed reference protein set annotation derived from GeneMarkS-2+ v6.10 (NCBI-PGAP) and BV-BRC v3.57.31 and Genome Quality Metrics.

Genomic Statistics	**Value**
Genome Length (bp)	2,594,120
GC content (%)	43.98
Genes (total)	2,574
CDSs (total)	2,515
Genes (coding)	2,442
CDSs (with protein)	2,442
Genes (RNA)	59
complete rRNAs	1, 1, 1 (5S, 16S, 23S)
tRNAs	53
ncRNAs	3
Pseudo Genes (total)	73
Pseudo Genes (ambiguous residues)	0 of 73
Pseudo Genes (frameshifted)	14 of 73
Pseudo Genes (incomplete)	54 of 73
Pseudo Genes (internal stop)	10 of 73
Pseudo Genes (multiple problems)	5 of 73
CRISPR Arrays	1 (Location: 1,336,297-1,337,389)
Genome Quality Metrics	
Contig L50	5
Contig N50	160075
Hypothetical CDS Ratio	0.4656
Coarse Consistency	97
Fine Consistency	95.9
CheckM Completeness	100
Genome Quality	Good

Table 2. The digital DNA-DNA hybridization (dDDH) results depict the genomic similarity between *Llb. buchneri* sp. *silagei* AGA55 and other closely related *Llb. buchneri* genomes, which were utilized for the ANI phylogram.

Reference genome	dDDH	Model C.I.	Distance	Prob. DDH >= 70%	GC difference
MGR2_32	97.90	[96.9 - 98.5%]	0.0033	97.83	0.36
S58	97.80	[96.9 - 98.5%]	0.0033	97.81	0.29
S59	97.60	[96.6 - 98.3%]	0.0036	97.78	0.16
NK01	97.40	[96.3 - 98.1%]	0.0039	97.73	0.02
177	96.90	[95.7 - 97.7%]	0.0045	97.62	0.23
CIRM_BIA_1516	96.80	[95.6 - 97.7%]	0.0045	97.61	0.10
CIRM_BIA_2081	96.70	[95.4 - 97.6%]	0.0047	97.58	0.04
CIRM_BIA_1514	96.40	[95.2 - 97.4%]	0.0050	97.53	0.17
SG162	96.00	[94.6 - 97.1%]	0.0055	97.44	0.09
MGB0786	78.10	[75.1 - 80.8%]	0.0257	88.95	0.52
RUG14303	77.90	[74.9 - 80.6%]	0.0258	88.83	0.60
ATCC4005	77.40	[74.4 - 80.1%]	0.0265	88.33	0.48
PC-C1	77.20	[74.2 - 79.9%]	0.0267	88.13	0.23
CIRM_BIA_2083	77.20	[74.2 - 80%]	0.0267	88.16	0.31
1014	77.10	[74.1 - 79.8%]	0.0269	87.99	0.36
DSM20057	77.00	[74 - 79.7%]	0.0270	87.93	0.43
CIRM_BIA_664	77.00	[74 - 79.7%]	0.0270	87.89	0.27
CIRM_BIA_845	77.00	[74 - 79.7%]	0.0270	87.9	0.27
CIRM_BIA_2084	76.80	[73.8 - 79.5%]	0.0273	87.7	0.01
LA1184	76.70	[73.7 - 79.4%]	0.0274	87.61	0.06
CIRM_BIA_2082	76.60	[73.6 - 79.4%]	0.0274	87.57	0.24
LA1167	76.30	[73.2 - 79%]	0.0279	87.16	0.11
LA1147	76.30	[73.3 - 79.1%]	0.0278	87.22	0.14
LA1161B	76.20	[73.2 - 78.9%]	0.0280	87.07	0.04
FUA3252	76.10	[73.1 - 78.8%]	0.0281	86.96	0.20
1012	75.80	[72.8 - 78.6%]	0.0284	86.71	0.08

Table 3. Prophage regions predicted in the *Llb. Buchneri* sp. *silagei* AGA55 genome using the PHASTEST webserver.

Region	Region Length	Completeness	Score	Total Proteins*	Region Position	Most Common Phage (Number of matching proteins)	GC %
1	46.6Kb	intact	140	66	181641-228252	PHAGE_Lactob_Lb_NC_047983(26)	39.59%
2	53.5Kb	intact	150	54	2048245-2101764	PHAGE_Lactob_Lb_NC_047983(8)	38.32%

*Protein counts reflect tool-predicted CDS within each region; values in the Supplementary Excel File correspond to CDS retained after reannotation, accounting for the difference.

Table 4. Antibiotic sensitivity patterns of *Llb. Buchneri* sp. *silagei* strain AGA55.

Antibiotic Group	Antibiotic	Zone Diameter (mm) /Status*
β-Lactams	Methicillin (5 µg)	Not detected (R)
	Penicillin G (10 U)	15,43±0,33 (I)
Aminoglucosides	Streptomycin (10 µg)	Not detected (R)
	Amikacin (30 µg)	Not detected (R)
	Kanamycin (30 µg)	Not detected (R)
Vancomycin	Vancomycin (30 µg)	Not detected (R)
Macrolides	Azithromycin (15 µg)	15,63±0,82 (I)
	Erthromycin (10 µg)	22,16±0,09 (S)
Tetracyclines	Tetracycline (30 µg)	20,26±0,30 (S)

Table 5. List of compounds identified in the CFS of *Llb. buchneri* sp. *silagei* strain AGA55, dissolved in Acetonitrile.

Peak	Retention time	Area (%)	Height (%)	A/H	Identified Compound from WILEY-NIST*	Mol.W. (g/mol)	Target and qualifier ion matches (m/z)
1	6,736	0,25	0,56	5,75	2-[(Trimethylsilyl)oxy] **propan-1-ol**	148	73, 75, 117
2	7,395	1,27	1,67	9,73	N,N'-dimethylbenzamidine	148	73, 147, 96
3	7,78	0,03	0,08	4,86	**Butanoic acid**, 3-methyl-2-oxo-, trimethylsilyl ester	188	73, 75, 117
4	8,048	6,91	13,82	6,39	**D-(-)-Lactic acid**, trimethylsilyl ester	162	73, 119
5	8,57	0,76	0,53	18,42	3-(1-Ethoxy-ethoxy)-**butan-1-ol**	162	73, 86, 117
6	8,69	0,34	0,57	7,73	**1-Pentyn-4-ol**, 1-(tert-butyldimethylsilyl)-	198	73, 75, 117
7	8,908	0,83	0,68	15,76	**Propanoic acid**, 2-hydroxy-, ethyl ester, (S)-	118	45, 75, 117
8	9,321	0,23	0,51	5,78	**Acetic acid**, (trimethylsilyl)- (CAS)	132	75, 117
9	12,905	1,22	0,82	19,07	**L-(+)-Lactic acid**, trimethylsilyl ether	182	75, 117
10	14,671	1,48	1,16	16,33	**Propanoic acid**, 3-(trimethylsilyl)-, ethyl ester	174	73, 75, 131
11	15,265	0,33	0,47	8,94	Trimethylsilyl **2-acetoxyacetate**	190	73, 75, 171
12	15,78	1,91	1,17	20,85	**L-(+)-Lactic acid**, trimethylsilyl ether	162	73, 75, 117
13	17,269	2,31	4,35	6,78	**D-Lactic acid**-DITMS	234	73, 117, 147
14	17,839	9,09	6,12	18,97	1-[(Trimethylsilyl)oxy]**propan-2-ol**	148	73, 75, 131
15	18,49	0,62	0,4	19,94	**Xylitol**	152	61, 101, 129
16	20,547	4,85	8,58	7,22	**L-(+)-Lactic acid**, tert-butyldimethylsilyl ester	204	73, 75, 119
17	23,015	0,86	1,02	10,87	**Butane**, 1,2,3-tris(trimethylsiloxy)-	322	73, 101, 117
18	23,465	0,56	0,35	20,33	2,3,4,5-Tetrahydro-1H-3-benzazepine	147	103, 117, 147
19	23,765	0,56	0,46	15,45	3,6-Dioxa-2,7-disilaoctane, 2,2,4,7,7-pentamethyl- (CAS)	220	73, 75, 117, 147
20	24,315	1,46	0,72	26,15	1,2-Dioxetane, 3,4,4-trimethyl-3-[[(trimethylsilyl)oxy]methyl]-	204	73, 103,131, 147
21	24,64	1,86	0,84	28,37	**D-Erythronic acid .gamma.-lactone**, bis(trimethylsilyl) ether	262	73, 103, 117, 147
22	25,253	11,45	15,53	9,42	Trimethylsilyl **2-acetoxyacetate**	190	73, 75, 117
23	25,556	1,2	0,82	18,64	**1-Butanol**, 3-t-butyldimethylsilyloxy-	204	73, 103, 117, 147
24	25,715	1,13	0,66	21,82	1,4-Dioxane, 2,5-bis[(trimethylsilyl)oxy]-	264	58, 101, 117
25	26,462	16,18	17,9	11,55	**Butane**, 1,2,3-tris(trimethylsiloxy)-	322	73, 101, 117
26	32,648	31,23	19,99	19,93	3,7-Dioxa-2,8-disilanonane, 2,2,8,8-tetramethyl-5-[(trimethylsilyl)oxy]- (CAS)	308	73, 103, 117, 147
27	60,365	0,33	0,06	71,81	2-Pyrrolidone-5-carboxylic acid, tert-butyldimethylsilyl ester	243	57, 84, 186
28	69,73	0,75	0,16	61,58	**Cyclo(L-Pro-L-Leu)****	210	70, 86, 154

*Due to derivatization, identified compounds were listed in their derivatized forms; most of the bold-marked compounds are expected to be released because of the metabolic activity of carbohydrate-active enzymes (CAZYmes).
**Non-ribosomally biosynthesized cyclic di-peptide.

Table 6. Probiotic characterization test results of *Llb. buchneri* subsp. *silagei* strain AGA55

Characterization Test	**Result**	
β-hemolysis on Blood Agar	Non-hemolytic	
Auto-aggregation (%)	81,60± 0,91	
Cell-surface hydrofobicity (%)	28,79±0,88	
Cholesterol assimilation (%)	37,04±2,08	
Antioxidant activity against DPPH (%)	73,14±0,81	
Antioxidant activity against $ABTS^{+}$(%)	73,03±0,26	
Survival behavior under static *in vitro* gastrointestinal digestion simulation		
Time*	**Log CFU/mL**	**Survival Rate (%)**
Hour 0. [in simulated gastric fluid (SGF)]	10,204	100
Hour 1. [in simulated gastric fluid (SGF)]	8,544	83,73
Hour 2. [in simulated gastric fluid (SGF)]	8,359	81,92
Hour 3. [in simulated intestinal fluid (SIF)]	9,498	93,083
Hour 4. [in simulated intestinal fluid (SIF)]	9,525	93,345
Antimicrobial activity test results		
Test strain	**Zone of inhibiton (mm)**	
Escherichia coli O157:H7 ATCC 43897	14,275±0,29	
Escherichia coli ATCC 25922	16,233±0,377	
Staphylococcus aureus ATCC 25923	17,525±0,420	
Bacillus cereus ATCC 33019	17,025±0,593	
Klebsiella pneumoniae ATCC 11883	15,633±0,612	

*SGF: contains 2000 U/mL pepsin and a working pH of 3.0; SIF: contains 10 mM bile salts, 100 U/mL pancreatin, and a working pH of 7.0. SGF and SIF have been prepared according to the "*INFOGEST static in vitro simulation of gastrointestinal food digestion*" protocol (Brodkorb et al., 2019).

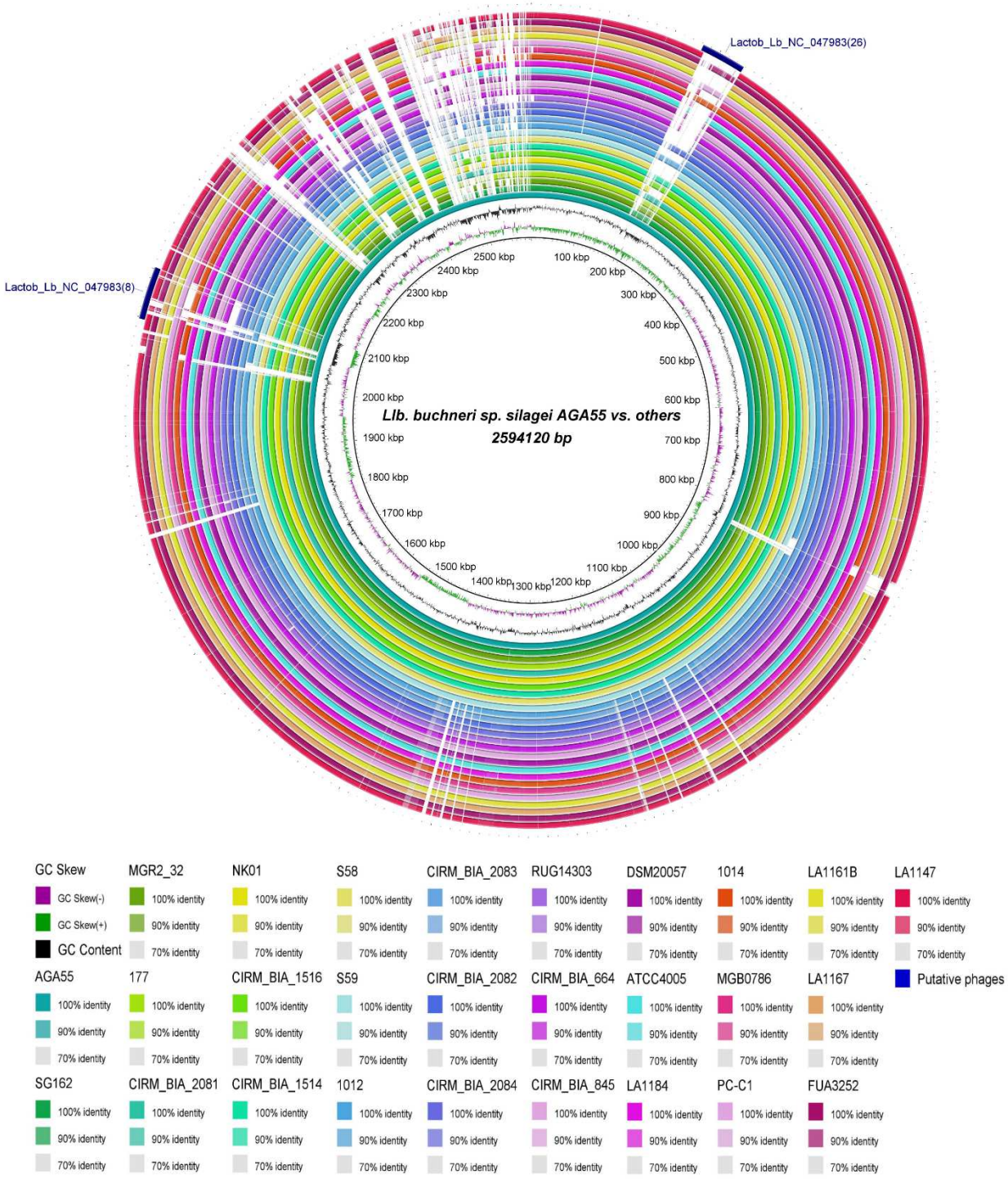

Fig. 1. BLAST ring image showing *Lentilactobacillus buchneri* genomes. The alignment starts at the inner dark turquoise ring (AGA55), located after the GC content, and extends to the outer dark pink ring (LA1147). The GC skew (+/−) of the AGA55 genome was displayed in the first inner circle from the ruler, while the GC content was illustrated in the second inner circle, which is after the GC skew. Moreover, the putative phage regions of the AGA55 genome were represented as navy blue arcs in the outer circle.

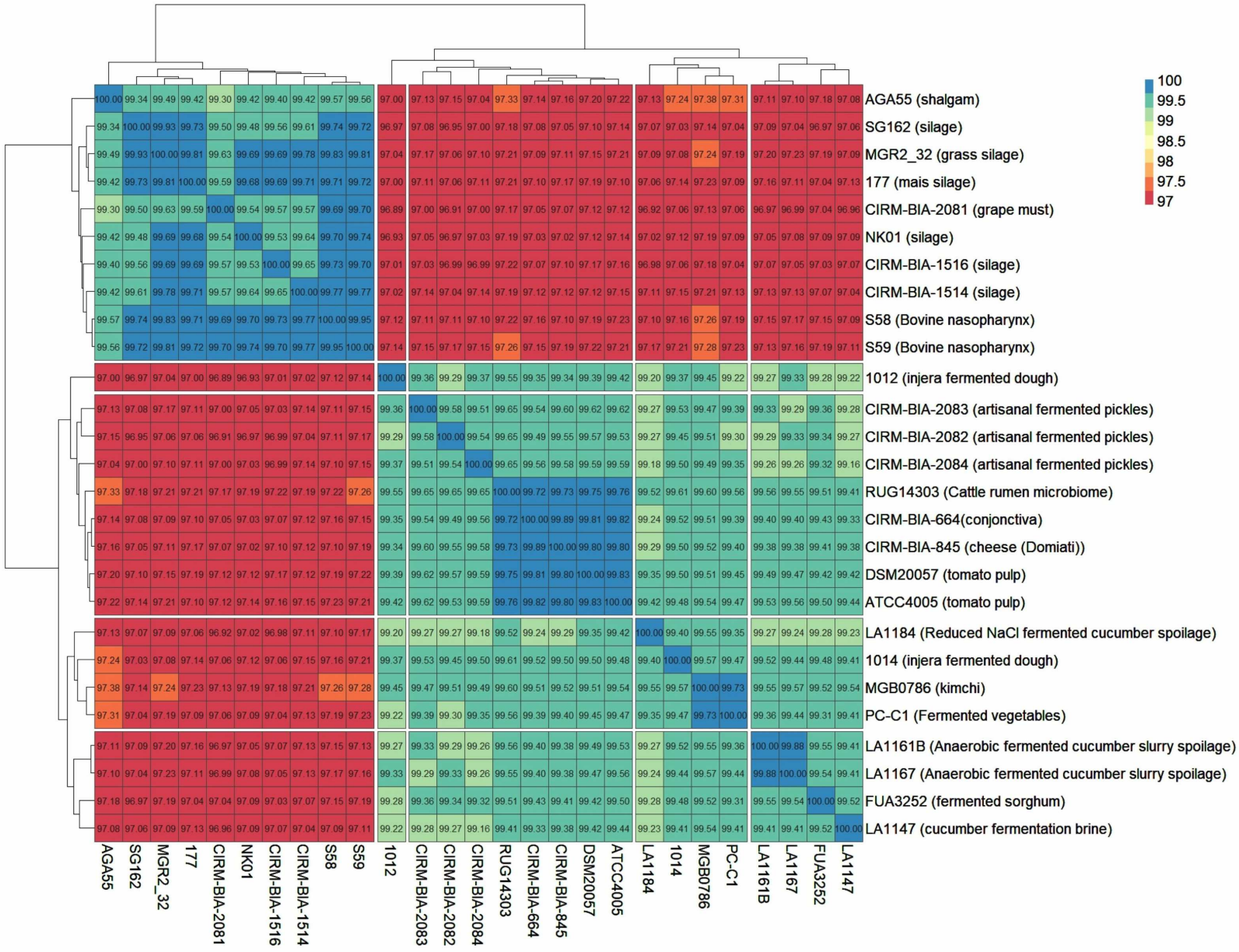

Fig 2. Average Nucleotide Identity (ANI) phylogram of *Lentilactobacillus buchneri* sp. *silagei* AGA55 compared to other existing *Lb. buchneri* genomes. ANI values have been calculated using the Fast ANI approach.

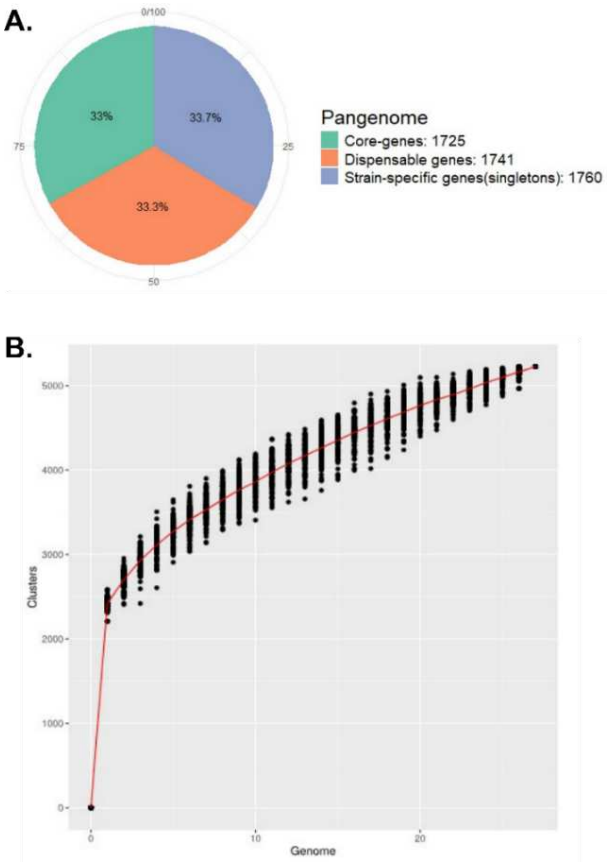

1182

1183 **Fig 3.** A: Distribution of the core-genes, dispensable genes and Strain-specific genes. B: The rarefaction curve
1184 generated by the Micropan R program represents the cumulative number of gene clusters (pangenomes) observed with
1185 an increasing number of genomes analyzed. Alpha value of 0.594107195589153 was calculated using the Heaps law
1186 approach described by Tettelin et al. (2008).

1187

1188

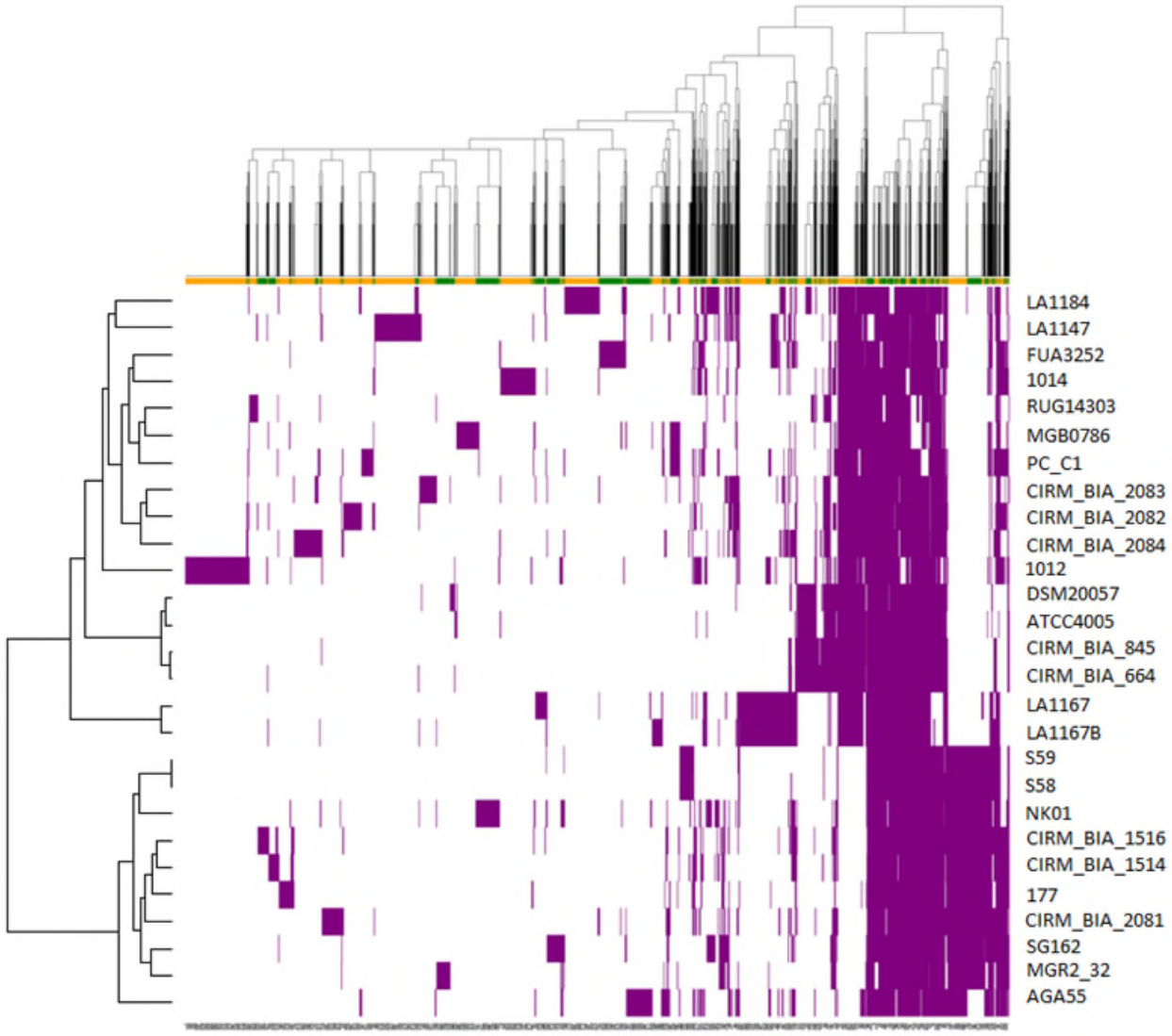

Fig 4. Matrix illustrating the presence or absence of clusterized genes. Genes are highlighted if present in the genomes. Gene clusters and genomes have been grouped via hierarchical clustering.

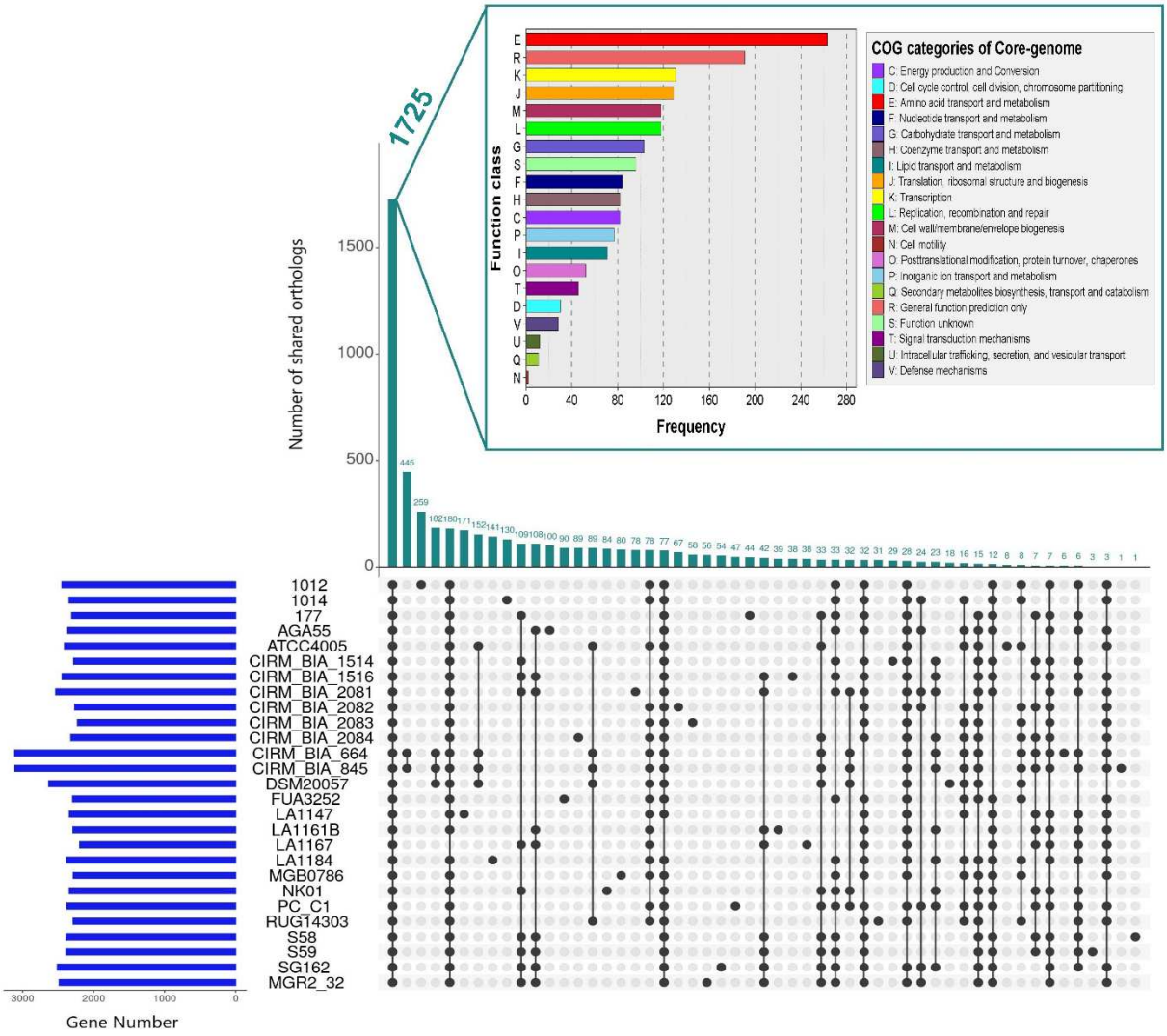

Fig 5. The Upset plot displays the quantity of core-genome, strain-specific (singletons), and other dispensable genes. Clusters of orthologous groups (COGs) linked to the core-genome are also shown in the Upset plot.

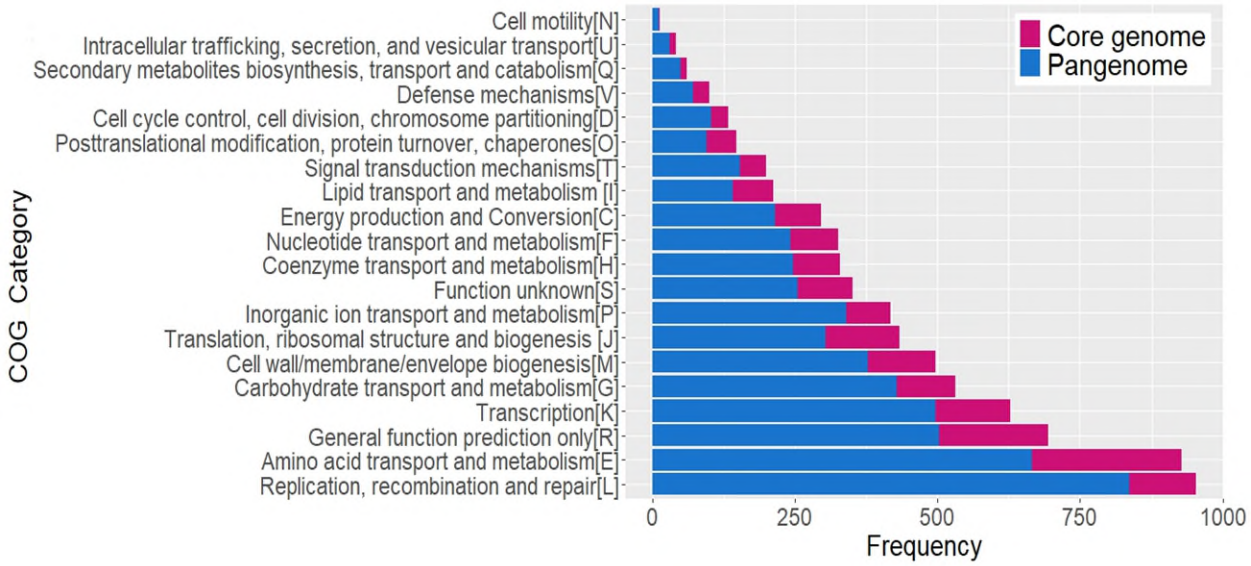

Fig 6. The number of COG categories observed in the core (red) and pangenome (light green) of twenty-seven genomes of *Lentilactobacillus buchneri*.

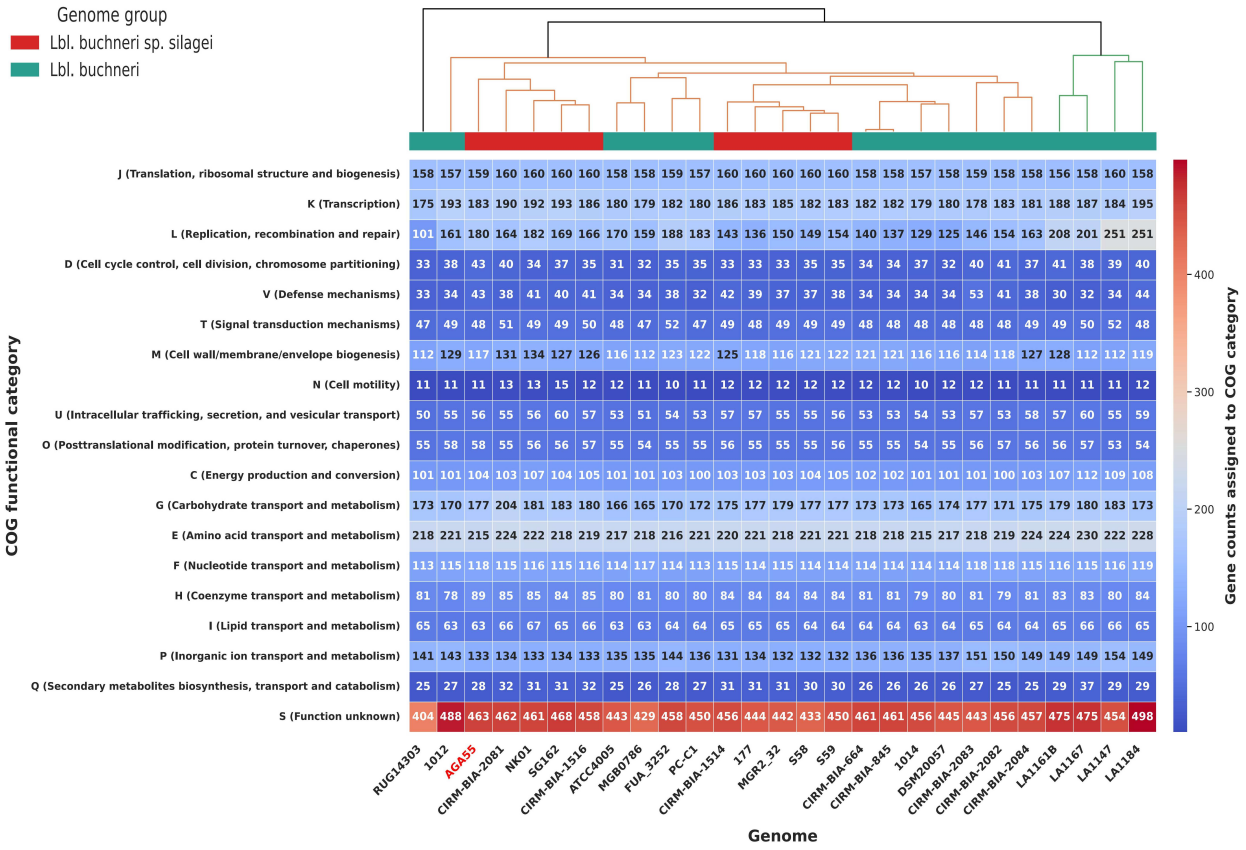

Fig 7. COG category heatmap of 27 *Lbl. buchneri* genomes. Cells show gene counts per COG functional category (number printed in each cell; color = count, coolwarm). Genomes (x-axis) are ordered by hierarchical clustering of COG profiles (Bray–Curtis, average linkage; dendrogram on top). The top color strip marks genome groups: *Lbl. buchneri* sp. *silagei* (red) and *Lbl. buchneri* (green). AGA55 is highlighted in red.

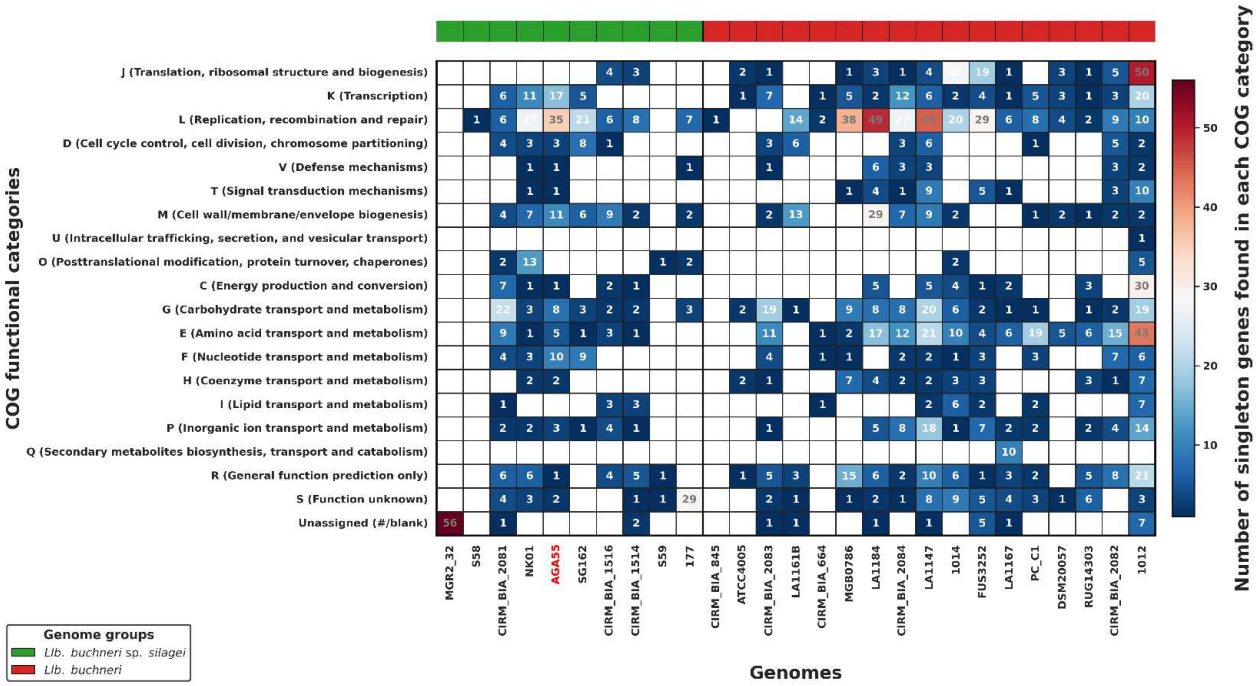

Fig 8. Heatmap of singleton (strain-specific) gene counts assigned to COG functional categories across Lentilactobacillus buchneri genomes. Values are shown in each cell; color indicates count (blue–red scale), and white indicates 0. Genomes are grouped by FastANI clustering (top bar: green = *Llb. buchneri* sp. *silagei*; red = *Llb. buchneri*), with the black vertical line marking the cluster boundary; AGA55 is highlighted in red in the x-axis labels. COG categories are labeled by letter and description; unassigned entries (blank/"#") are labeled Unassigned.

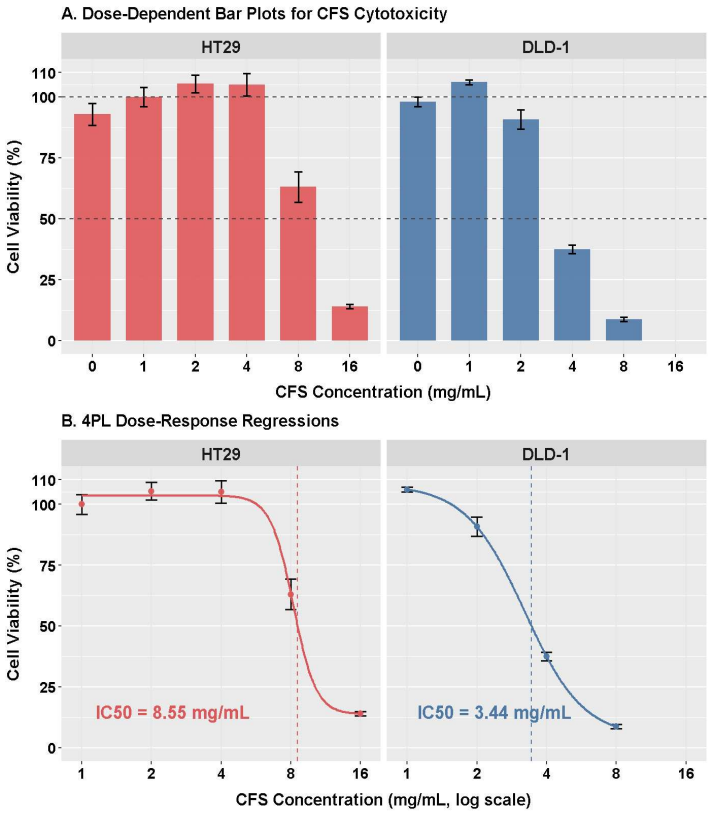

1260

1261 **Fig 9.** The CCK-8 assay results were derived from the analysis of cell-free supernatants (CFS) of *Lentilactobacillus*
1262 *buchneri* subsp. *silagei* AGA55 on the HT29 and DLD-1 colorectal adenocarcinoma cell lines; 0 mg/mL CFS indicates
1263 the sample devoid of CFS. A represents cytotoxicity of different CFS concentrations while B shows dose-response
1264 curves (4PL fit) with IC50 value.

1265

1266

1267

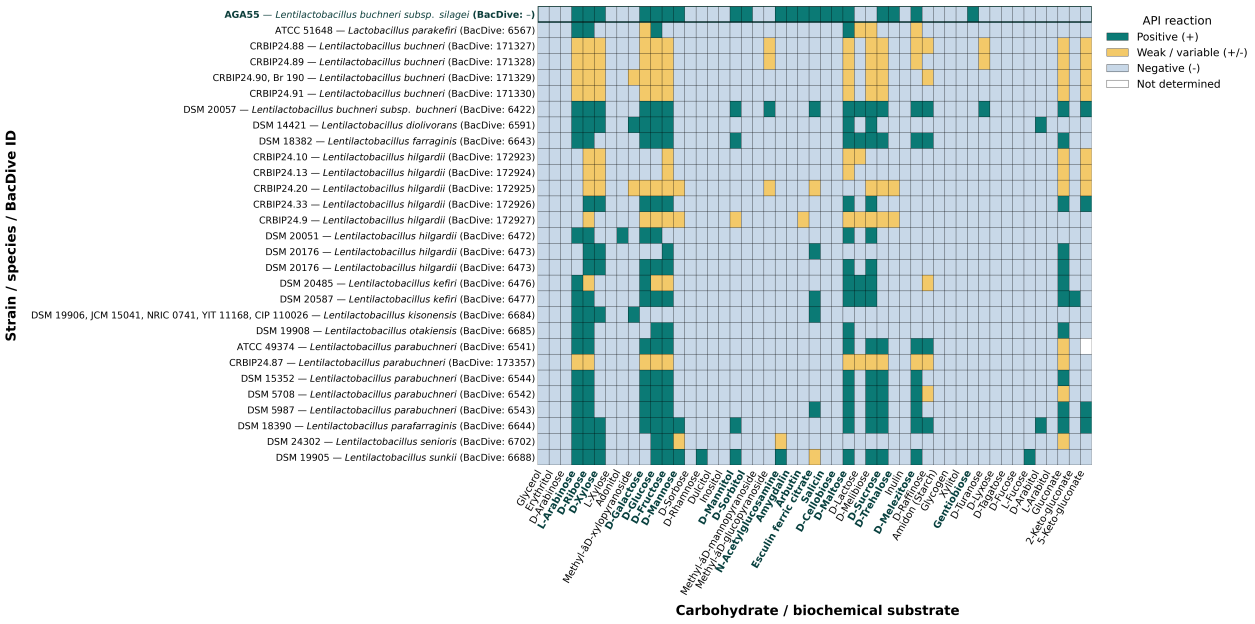

Fig 10. Heatmap showing carbohydrate substrate utilization patterns for strain AGA55 and *Lentilactobacillus* reference strains retrieved from BacDive. Rows represent bacterial strains, indicated by collection number, species name, and BacDive identifier where available. Columns represent individual carbohydrate or biochemical substrates included in the API 50 CH panel. Reaction outcomes are color-coded as follows: positive fermentation reactions (+) are shown in teal, weak or variable reactions (+/-) are shown in yellow, negative reactions (−) are shown in light gray, and not determined values are shown in white. The carbohydrate labels corresponding to positive reactions in AGA55 are shown in bold.

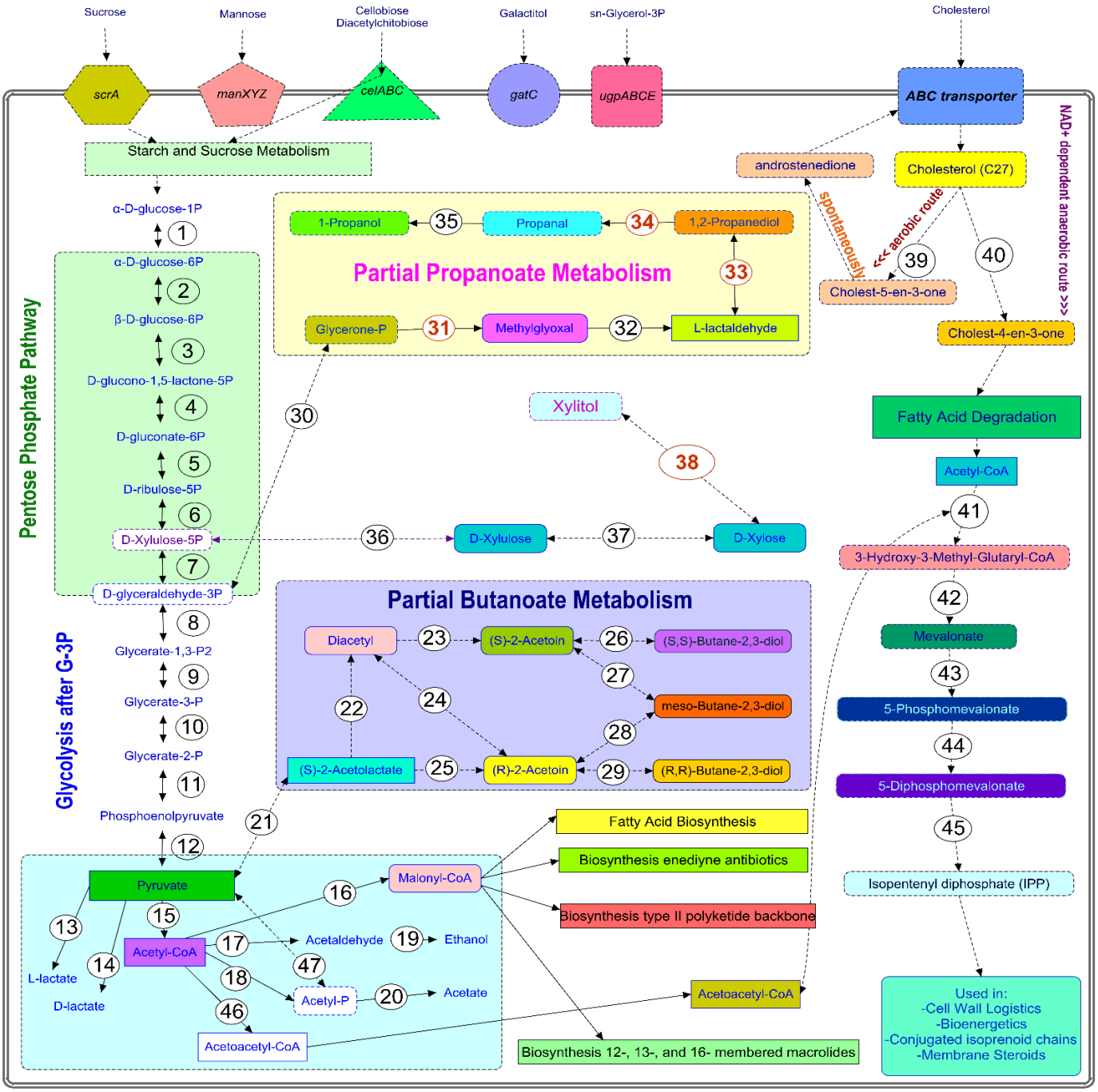

Fig 11. Putative summary of pyruvate and cholesterol metabolic pathways as predicted from KEGG and MetaCyc via JGI/IMG-MER. 1: phosphoglucomutase (*pgm*, K01835/EC:5.4.2.2), 2: glucose-6-phosphate isomerase (*pgi*, K01810/EC:5.3.1.9), 3: glucose-6-phosphate 1-dehydrogenase (*zwf*, K00036/EC:1.1.1.49, 1.1.1.363), 4:6-phosphogluconolactonase (*pgl*, K07404/ EC:3.1.1.31), 5:6-phosphogluconate dehydrogenase(*gntZ*, K00033/ EC:1.1.1.44, 1.1.1.343), 6:ribulose-phosphate 3-epimerase(rpe, K01783/ EC:5.1.3.1), 7: xylulose-5-phosphate/fructose-6-phosphate phosphoketolase (*xpk*, K01621/EC:4.1.2.9, 4.1.2.22), 8:glyceraldehyde 3-phosphate dehydrogenase (phosphorylating, gapA, K00134/EC:1.2.1.12), 9: phosphoglycerate kinase (pgk, K00927/ EC:2.7.2.3), 10: 2,3-bisphosphoglycerate-dependent phosphoglycerate mutase (*gpmA*, K01834/EC:5.4.2.11), 11: enolase1/2/3 (*eno*, K01689/EC:4.2.1.11), 12: pyruvate kinase (pyk, K00873/EC:2.7.1.40), 13:L-lactate dehydrogenase (*ldh*, K00016/ EC:1.1.1.27), 14: D-lactate dehydrogenase(*ldhA*, K03778/EC:1.1.1.28), 15: pyruvate dehydrogenase (EC 1.2.4.1 > 2.3.1.12), 16: acetyl-CoA carboxylase carboxyl transferase (K01961,K01962,K01963,K02160), 17: acetaldehyde dehydrogenase / alcohol dehydrogenase (*adhE*, K04072/EC:1.2.1.10, 1.1.1.1), 18:phosphate acetyltransferase (*pta*, K00625/ EC:2.3.1.8), 19: alcohol dehydrogenase (K04072, EC 1.1.1.1), 20: acetaldehyde dehydrogenase (K04072, EC:1.2.1.10), 21:acetolactate synthase I/II/III large subunit (K01652, EC:2.2.1.6), 23: diacetyl reductase(K03366/EC 1.1.1.304), 24: (R,R)-butanediol dehydrogenase / diacetyl reductase(K00004 / 1.1.1.303), 25: acetolactate decarboxylase (K01575, EC:4.1.1.5), 26: (S,S)-butanediol dehydrogenase (K03366/ EC 1.1.1.76), 27-28: meso-butanediol

dehydrogenase (K00004/EC:1.1.1.-), 29: (R,R)-butanediol dehydrogenase (K00004/EC:1.1.1.4), 30: triosephosphate isomerase (K01803/ EC:5.3.1.1), 31: Not detected via KEGG and MetaCyc, 32: lactaldehyde dehydrogenase(MetaCyc: PWY-5458/EC:1.2.1.22), 33: Not detected via KEGG and MetaCyc, 34: alcohol dehydrogenase (propanol preferring, PWY-7013/ EC:1.1.1.1), 35: 1,3-propanediol dehydrogenase (*dhaT*, K00086/ EC:1.1.1.202), 36: xylulokinase (*xylB*,K00854/EC:2.7.1.17), 37:xylose isomerase (*xylA*, K01805/EC:5.3.1.5), 38: detected via GC-MS but not predicted via KEGG and MetaCyc, 39: cholesterol oxidase (MetaCyc: PWY-6945), 40: cholesterol dehydrogenase (MetaCyc:PWY-6946), 41: hydroxymethylglutaryl-CoA synthase (PWY-922/K01641/EC:2.3.3.10), 42: hydroxymethylglutaryl-CoA reductase (PWY-5074/ K00054/EC:1.1.1.88), 43: mevalonate kinase (PWY-922/K00869/EC:2.7.1.36), 44: phosphomevalonate kinase (PWY-922/ K00938/ EC:2.7.4.2), 45: diphosphomevalonate decarboxylase (PWY-922/ K01597/EC:4.1.1.33), 46: acetyl-CoA C-acetyltransferase (K00626/ EC:2.3.1.9), 47: pyruvate oxidase(K00158/ EC:1.2.3.3).

Supplementary Files

This is a list of supplementary files associated with this preprint. Click to download.

- SUPPLEMENTARYMATERIALS.pdf
- SupplementalExcelFile.xlsx